Unified theory of linear instability of anisotropic surfaces and interfaces under capillary, electrostatic, and elastostatic forces: The regrowth of epitaxial amorphous silicon

Tarik Omer Ogurtani*
Department of Metallurgical and Materials Engineering, Middle East Technical University, 06531, Ankara, Turkey
(Received 13 May 2006; revised manuscript received 21 July 2006; published 20 October 2006)

The first-order unified linear instability analysis (LISA) of the governing equation for the evolution of surfaces and interfaces under capillary, electromigration (EM), and elastostatic forces is developed. A formal treatment of the thermomigration (Soret effect) driven by the nonuniform temperature distribution caused by exothermic phase transformation (growth) at the surface and interfacial layers is presented and its apparent influence on the capillary force in connection with the stability is also established in a concise analytical form. This unified approach, which relies on a rigorous theory of irreversible thermodynamics of surfaces and interfaces, seriously considers the anisotropies associated with the generalized growth mobility, the interfacial specific Gibbs free energy (i.e., the surface stiffness), and the surface diffusivity in thin solid films. The singularity in the surface stiffness at the cusp regions of the Wulff construction of the surface Gibbs free energy is fully elaborated by using a modified cycloid-curtate function as a basis for generating the Dirac δ distribution, which shows an unusually strong anomalous effect on the surface morphological instability even in the absence of EM forces, as illustrated clearly by the graphical representation of the EM-induced instability threshold level as a function of tilt angle and wave number, in a three-dimensional plot for various intrinsic and normalized system parameters. In the development of LISA theory special attention is paid to the origin of the elastostatic forces, which include not only the elastic strain energy density, but also the elastic dipole tensor interaction between mobile atomic species and the applied stress field. The profound influence of the anomalous surface stiffness anisotropy on the surface morphological evolution under the applied stress system is demonstrated by three-dimensional computer graphics applied for copper and silicon thin single-crystal solid films having, respectively, sixfold {111}- and fourfold {100}-symmetric singular (vicinal) planes as the top surfaces, which reveal the fine features of the theory and give insight into some controversial issues related to LISA in the literature. This unified approach also considers the stress dependence of the generalized growth mobility and its profound influence on the stability of the interface displacement and roughening in thin solid films. As a special application of the theory, the effects of uniaxial and biaxial applied stresses on the recrystallization and the interfacial morphological evolution of amorphous Si deposited on silicon substrates are thoroughly analyzed and excellent quantitative agreement is found with the published experimental data in the literature.

DOI: 10.1103/PhysRevB.74.155422 PACS number(s): 68.35.Md, 85.40.Ls, 66.30.Qa, 05.70.Np

I. INTRODUCTION

For many years, the subject of capillary-driven morphological evolution at the surfaces and interfaces of crystalline solids, especially under the action of applied force fields such as electrostatic and thermomechanical stress systems, has represented a challenging theoretical problem in materials science, without having been exposed to any robust nonequilibrium thermodynamic treatments in crystalline solids, which is just the opposite of the case of fluid systems, where highly sophisticated nonequilibrium thermodynamic theories, advocated originally by Bedeaux,[1] having quite a different context and objectives, are available in the literature.[2,3] This situation has started to change very recently,[4–6] because the submicroscopic nature of electronic devices has pushed surfaces and interfaces into the front lines as primary agents in the determination of the catastrophic failure of the interconnected thin metallic lines used in microelectronic industries. Similarly, in the last two decades, the invention of the scanning tunneling microscope (STM) has simulated studies of nanoscale activities on solid surfaces. The most interesting finding is the self-assembly of monolayer atoms on solids surfaces into nanoscale features.[7,8]

Theoretical studies of interconnected surfaces under the electromigration force have also revealed a variety of morphological scenarios. Krug and Dobbs[9] and Schimschak and Krug[10] showed that a crystal surface can be destabilized by an external electromigration (EM) field in a material having anisotropic adatom surface diffusivity. Their linear instability analysis (LISA) strictly relies on uniformly tilted surfaces and/or small slope approximations, respectively. They also assumed that the field is almost constant along the surface. Nevertheless, it may be instructive to explore several aspects of the morphological instability of crystal surfaces and faceting transitions. Later studies undertaken by Schimschak and Krug,[11] Gungor and Maroudas,[12] and Ogurtani and Oren[13] put more emphasis on the crucial role of surface diffusion anisotropy and crystalline texture[14] in the development of the unusual morphological variations of preexisting edge or internal voids causing catastrophic electrical breakdown. The latter authors also successfully studied the intergranular motion of internal voids in "bamboo" metal lines, which has received scant attention in the literature as mentioned in a recent paper by Nathan *et al.*,[15] who performed exploratory computer simulations of the EM-induced surface evolution with transgranular and intergranular edge voids assuming

that the triple junction (TJ) sustains its equilibrium configuration. They also observed that the EM forces slow down the development of an intergranular groove along the positively tilted grain boundary (GB).

Very recently, Ogurtani and Akyildiz[16,17] have observed the profound effects of the reflecting and/or free-moving boundary conditions on EM-induced grain boundary grooving (GBG) and cathode voiding in their computer simulation studies. These computer experiments showed irrevocably that in the electromigration-dominating regime GB voiding can be completely arrested by applied current above the well-defined threshold level and the dynamical dihedral angles rotate gradually towards the windward side while keeping their angular difference invariant, but having fine-scale random fluctuations due to the strong nonlinear connectivity associated with global entropy production.

Bradley[18] examined the effects of electromigration on the dynamics of corrugated interconnect-vapor interfaces using a multiple-scale asymptotic analysis by neglecting the capillary effects. This very powerful technique was first introduced by Drazin and Johnson[19] to deduce the governing Korteweg–de Vries (KdV) equation for the irrotational two-dimensional (2D) motion of an incompressible inviscid fluid. During the derivations of the KdV equations by Drazin and Johnson[19] and Bradley[18] very special initial data for the nonlinear partial differential equation are chosen in order to get the solitary-wave solution, which represents at the limit a highly hypothetical and physically unobservable disturbance on the surface. This compressed and highly stretched solitary wave travels on the surface of a current-carrying metallic thin film in the direction of the applied EM field. The propagation velocity and the width of the solitons decrease with increasing amplitude. The most interesting work on the EM-induced edge stability in single-crystal metal lines was carried by Mahadevan *et al.*[20] They employed a phase field (PF) technique to study this moving-boundary problem numerically by assuming that the mobility of an adatom is anisotropic, having fourfold symmetry with a 45° tilt angle. Mahadevan *et al.*[20] showed that if the applied current density is below the threshold level, the notch smoothes away in the course of time; otherwise, the perturbation produces an edge instability and grows to become a slit-shaped void propagating at 45° to the line edge.

The most recent and thorough linear instability analysis of the surface topological evolution affected by the electromigration and capillary forces alone has been performed by Brush and Oren utilizing a governing equation, which was originally derived by Ogurtani[21] using a rigorous microdiscrete formulation of the irreversible thermodynamics of surfaces and interfaces. This approach has produced very rich information on the electromigration-induced surface instabilities and the limitations and validity of the LISA theory in the prediction of stability requirements in the case of finite-size periodic surface modifications.

The stability of the stressed solid surfaces under a variety of environmental conditions still today is a challenging theoretical problem. Asaro and Tiller[22] made a first serious attempt to develop an equilibrium thermodynamic model of interfacial morphological evolution during stress corrosion cracking by adding the elastic strain energy density (ESED) directly to the chemical potential defined only at the surface. Unfortunately, like most authors, the ESED appears with a wrong sign in their formula. As shown by Ogurtani and Oren[5] the main reason for this sign conflict in the literature is due to the fact that starting with Herring,[23] the interface displacement process has been treated as an isothermal reversible process by minimizing the total Helmholtz free energy $\delta F=0$, rather than the dissipation function approach for nonequilibrium processes as indicated by Guggenheim[24] for natural isothermal processes, without imposing any volumetric constraints on the composite system. This nonequilibrium approach puts the generalized Gibbs free energy back into the front line for natural isothermal processes, and strangely enough the strain energy density enters into this characteristic function with a *negative sign*,[5,13] especially in those majority of cases where the stress dependence of the entropy density is almost negligible.[25] Since the appearance of any surface disturbances, in first order, regardless of the wave number decrease, the elastic strain energy density[26] consequently causes an equal amount of increase in the Gibbs free energy density of the bulk phase, which would then be an unnatural isothermal change that can never take place in nature.[24] One should also mentioned here that the sign conflict in the strain energy density also appears in other authors' studies related to the interfaces and triple junctions, notably Rice and Chuang,[27] Suo and Wang,[28] and Gungor and Maroudas,[29] who all base in their work on the equilibrium treatment of Herring.[23]

Later studies of Srolovitz[30] first considered a stress applied to the solid in the direction nominally in the plane of the interface. He tried to adapt the chemical potential by referring the work of Herring[31] on stress-assisted grain boundary diffusion, which considers only the stress normal to the surface. Srolovitz[30] proceeds alone the line of Asaro and Tiller[22] by dropping Herring's formula, which does not contribute to the traction-free solid surfaces, and rather adding the elastic strain energy density to the chemical potential directly. There are also some inconsistencies in their formulations[22,30] of the trace and the deviatoric part of the 2D stress tensor even though the hoop stress is correct, which can be easily detected by comparing them with the calculation of Gao,[32] who utilized the more sophisticated method of Muskhelishvili[33] in a 2D complex representation, successfully. That problem in the trace yields a sign conflict in the calculation of the stress-assisted bulk drift diffusion. All these models not only suffer from the sign conflict (the healing effect of rough surfaces is now replaced by the surface instability) but also predict identical behavior for solids under tension and compression in contradiction to some recent experimental results under etching,[34] because stress enters through the elastic strain energy density quadratically.

Hillig and Charles[35] and Chuang and Fuller[36] realized that the ESED contribution to the driving force is inadequate to explain the experimental findings. They postulated an *ad hoc* reaction kinetic theory, where the activation energy depends on the applied stress system through a fictitious activation strain, which is still an ill-defined and obscure quantity. Spencer *et al.*[37,38] made an extensive analysis of the morphological instability of growing epitaxially strained dislocation-free solid film based on the surface diffusion driven by the

stress-dependent chemical potential, where the elastic strain energy density again appears to be additive (sign conflict) in the so-called chemical potential like almost all other investigators mentioned previously, including Grinfeld.[39] They found that the critical film thickness for instability depends on the growth rate of the film itself, and they claimed that there are no stable nonlinear steady-state solutions that can be described by long-wave theory. Lu *et al.*[40] have measured the pressure dependence of the solid-phase epitaxial growth (SPEG) rate of self-implanted Si (100) in the temperature range of 530–550 °C and pressure up to 3.2 GPa (32 kbar). They found that the growth rate is enhanced by a factor of 5 over that at 1 bar atmospheric pressure and the measured activation volume is negative, about −28% of the atomic volume. Later Aziz *et al.*[41] studied the motion of the interface between crystalline and amorphous silicon (100) under the nonhydrostatic stress system. They have observed that the SPEG growth rate on the tensile side is greater than on the compressive side of elastically bent wafers. They have developed an activation strain tensor concept in connection with the kinetic expression using the technique advocated by Rice,[42] which has certain pinholes in the definition and usage of the Helmholtz and Gibbs free energy densities in contrast to the Gibbs chemical thermodynamics and further assuming that strain and stress are homogeneous functions of space. Barviosa-Carter *et al.*[43] have studied the effect of the in-plane stress system on the rate of growth of SPEG and the morphological instability of the corrugated Si (001) interface. They also performed computer simulations relying on an *ad hoc* kinetic formula based on empirical information and found that the corrugated interface is stable under tension and roughens under compression.

The anisotropy in the reaction mobility can come directly from the entropy of the activated complex, $\exp(\Delta S^*/k)$, which corresponds to the *steric* or *probability factor*, formally introduced in the theory of activated collisions in chemical reactions.[44] The steric factor is closely related to the probability of occurrences of certain atomic temporal configurations in the vicinity of the saddle point, such that the hopping attempt by the activated complex, having enough kinetic energy to surmount the barrier, becomes a successful jump. In fact, measurements by Csepregi *et al.*[45] of the epitaxial regrowth rate of crystalline Si from Si-implanted amorphous Si (SPEG) shows that the growth rate has a well-defined activation energy of 2.35±0.1 eV, which does not show any dependence on the orientations of the ⟨111⟩, ⟨110⟩, ⟨100⟩, and ⟨511⟩ directions. Since these experiments have been done on unstrained flat samples, they clearly indicate that the growth rate anisotropy has nothing to do with the surface Gibbs free energy and the elastic dipole tensor interaction (EDTI) anisotropy either. Therefore, it is directly connected to the mobility through the steric or activation entropy factor as we pointed out above. While adapting the same kinetic theory in their stability analysis, Liang and Suo[46] stated clearly that there is no *a priori* information available regarding the sign of the activation strain tensor in a given reaction and its connection with any mobile point-defect configuration. They also employed a quasithermodynamics treatment of the lump system, using an obscure concept such as the free energy, without paying any attention to the restrictive mathematical definitions of the characteristic functions (Gibbs, Helmholtz, energy, etc.) in Gibbs chemical thermodynamics[24] using like most authors straight additivity in their formulation of the various ill-defined energy contributions, having completely different thermodynamic characteristics, to the so-called the total free energy of the system including the surface, the ESED in their driving force expression appears with an improper sign. Then they claimed that this contribution alone destabilizes the surface roughness. Close inspection shows that they are actually using not even the Helmholtz free energy variation but the minimum internal energy criterion $\delta U=0$, which is a valid thermodynamic characteristic function for isochoric ($\delta V=0$) and adiabatic (isentropic, $\delta S=0$) processes. Furthermore, Liang *et al.*[46] adapted in their analysis an *ad hoc* kinetic law, which is first obtained empirically and later improved by some transition-state theoretical considerations. In the work of Liang *et al.*[46] and Barviosa-Carter *et al.*,[47] besides misspelling the sign of the ESED contribution to the driving force, there are some additional shortcomings related to arguments of the function representing their kinetic equation.

It is the main objective of the present paper to furnish a unified and tractable mathematical model of the linear stability theory of surfaces and interfaces, which can be easily adapted for computer simulations to deal with the above-cited intricate problems by only relying on the rigorous mesoscopic nonequilibrium thermodynamics of surfaces and interfaces[5,6] combined with the well-accepted hypothesis of the transition-state theory of reaction kinetics. In Secs. III and IV the predictions of the LISA theory are thoroughly furnished by unique and sound analytical expressions, which are supported by 3D computer graphics, while they are compared with the available experimental observations, and we find excellent agreement between them.

II. PHYSICAL AND MATHEMATICAL MODELING

According to the microdiscrete formulation of the irreversible thermodynamics of surfaces and interfaces, which was extensively elaborated and applied by Ogurtani[6,48] and Ogurtani and Oren[4,5] for multicomponent systems, the evolution kinematics of surfaces or interfacial layers (the generalized cylindrical surfaces in 3D space) may be described by the well-posed moving-boundary value problem in 2D space for ordinary points in terms of normalized and scaled parameters and variables.

In the present enlarged rigorous formulation, which may formally cover the *thermomigration* or so-called thermal drift diffusion known also as the Soret effect[49] in condensed states, the full emphasis is given to the effects of the applied stress system on the growth kinetics and the instabilities associated with the morphological evolution of anisotropic surfaces and interfaces. The anisotropic parts of the surface drift diffusion and the surface-specific Gibbs free energy of the interfacial layer are represented by the angular-dependent prefactors $D(\theta,\phi;m)$ and $\gamma(\hat{\theta},\hat{\phi};m)$, respectively. The angles θ and ϕ (tilt angle) give the orientations of the local tangent vector of the surface contour line in 2D space and the principal axis of the diffusion dyadic, which coincides with

one of the crystallographic directions, with respect to the x axis of the global Cartesian coordinate system. For this simple geometric construction, one assumes implicitly that the sidewalls and/or upper and lower surfaces of the single-crystal thin-film specimens coincide with one of those lower-Miller's index crystalline planes such as {100}, {110}, and {111} in faced-centered-cubic (fcc) structures. Similarly, the angle $\hat{\theta}$ measures the inclination of the local surface normal over which drift diffusion is taking place with respect to the same reference system. $\hat{\phi}$ is the tilt angle of the surface normal of the arbitrarily chosen vicinal crystallographic plane with respect to the x axis. Here $n=2m$ takes the set of numbers $\{n=2,4,6\}$ for fcc structures and represents the degree of folding $(2\pi/n)$ or the order of the rotational symmetry operation. The rotational symmetry axis that is characterized by the symbol C_n corresponds to the zone axis of a set of planes and coincides with the surface normal vector associated with one of the low-index crystallographic plane (singular-vicinal planes), making up the sidewalls and/or upper and lower surfaces of the single-crystal thin films.

The governing equation for the surface evolution may be rewritten in the following explicit form by assuming that the diffusing species are isotropic (monovacancy or self-interstitial mechanisms) and, therefore, they can only interact with the hydrostatic part of the stress tensor, $\hat{I}\,\mathrm{Tr}\,\underline{\underline{\sigma}}/3$ (see the Appendix). Hence, the stress-field–elastic-dipole interaction energy may have the following simplification in the case of isotropic stress-assisted diffusion: $u_{EDI}=-\Omega_\sigma \underline{\underline{\lambda}}_a \otimes \underline{\underline{\sigma}} \rightarrow -(1/3)\Omega_\sigma\,\mathrm{Tr}\,\underline{\underline{\lambda}}_a\,\mathrm{Tr}\,\underline{\underline{\sigma}}$. Here $\underline{\underline{\lambda}}_a$ is the effective elastic dipole tensor of the mobile atomic species, which is described in our previous publication[13] thoroughly. The stress-affected phase transformation mobility $\bar{M}_{bv}(\underline{\underline{\sigma}},\beta;T)$, which depends on the temperature exponentially (Arrhenius connection), as in the case of the recrystallization of amorphous Si, may also be dependent on the orientation of the interface, represented by the angle β with respect to the $\langle 100\rangle$ direction. Keeping all these possible complications in mind, one may write the following enlarged expression for the interface displacement velocity including the phase transformation in normalized and scaled space and time domain:

$$\bar{V}_{ord}=\frac{\partial}{\partial\bar{\ell}}\Bigg[\bar{D}(\theta,\phi;m)\frac{\partial}{\partial\bar{\ell}}[\Delta\bar{g}_{bv}+\chi\cdot\bar{\vartheta}+\Xi_\sigma\,\mathrm{Tr}\,\underline{\underline{\bar{\sigma}}}_{b/\sigma}-\Upsilon_\sigma\bar{T}_\sigma+\bar{\tilde{\gamma}}(\hat{\theta},\phi;m)\bar{\kappa}]\Bigg]-\bar{M}_{bv}(\sigma,\beta;T)[\Delta\bar{g}_{bv}+\bar{\tilde{\gamma}}(\hat{\theta},\phi;m)\bar{\kappa}]+\bar{M}_b\Xi_b\hat{n}\cdot\bar{\nabla}_2(\mathrm{Tr}\,\underline{\underline{\bar{\sigma}}}_{b/\sigma})-\bar{M}_b\Upsilon_b\hat{n}\cdot\bar{\nabla}_2(\bar{T}),\tag{1}$$

where $\bar{T}=T/T_m$ is the homologous temperature associated with the steady-state temperature distribution due to the Joule heating as well as the heat evolution during the exothermic phase transition taking place at the surface and/or interfacial layer. Υ_σ and Υ_b are dimensionless parameters and may be called the *thermomigration intensity* factors, which are, respectively, associated with the surface layer and the bulk phase, which will be defined later in this section. The last two terms in the above expression represent the stress and temperature gradient-assisted particle bulk drift diffusion to the interfacial layer, which eventually may contribute to the surface layer displacement, where $\bar{\kappa}$ is the local curvature and is taken to be positive for a concave solid surface (troughs) and negative for a crest. In our adapted convention, the line normal $\hat{n}$ is always directed towards the solid bulk region and the normalized interface displacement velocity at the ordinary points is given by $\vec{\bar{V}}_{ord}=\hat{n}\bar{V}_{ord}$. Here $\bar{\ell}$ is the curvilinear coordinate along the surface (arc length), $\bar{\nabla}_2$ is the gradient operator in the 2D scaled space with respect to ℓ_0, χ is the electron wind intensity (EWI) parameter, and $\bar{\vartheta}$ is the normalized electrostatic potential generated at the surface layer due to the applied electric field intensity. $\Delta_{bv}\bar{g}\Rightarrow\Delta\bar{g}_{bv}=(\bar{g}_v-\bar{g}_b)$ by definition is the volumetric Gibbs free energy density of transformation (GFEDOT) ($\Delta\bar{g}_{bv}<0$, evaporation; $\Delta\bar{g}_{bv}>0$, condensation) normalized with respect to the minimum value of the specific surface Gibbs free energy of the interfacial layer denoted by g_σ^0, where Δ_{bv} is the forward difference operator as is defined above implicitly. $\bar{M}_{bv}(\underline{\underline{\sigma}},\beta;T)$ is the normalized temperature- and stress-dependent generalized transformation mobility (i.e., recrystallization or condensation). The stress and orientation dependence of $\bar{M}_{bv}$ is formulated by the author using a transition-state theoretical argument, which will be fully elaborated in Sec. V. In this paper v represents the realistic void region, which contains a fluid phase including the amorphous solid state that shows rapid shear strain relaxation (high fluidity) compared to the mass flow due to drift diffusion along the boundary layer at the test temperatures.

In the present enlarged formulation of the problem, an overbar still indicates the following scaled and normalized quantities:[50,51]

$$\bar{t}=t/\tau_0,\quad \bar{\ell}=\ell/\ell_0,\quad \bar{\kappa}=\kappa\ell_0,\quad \bar{w}_0=w_0/\ell_0,\tag{2}$$

$$\bar{L}=L/\ell_0,\quad \Upsilon_{\sigma,b}=\frac{s_T^{\sigma,b}T_m\ell_0}{\Omega_\sigma g_\sigma^0},$$

$$\Delta\bar{g}_{bv}=\frac{\breve{g}_{bv}\ell_0}{g_\sigma^0},\quad \bar{\vartheta}=\frac{\vartheta}{E_0\ell_0},\quad \chi=\frac{e|\hat{Z}|E_0\ell_0^2}{\Omega_\sigma g_\sigma^0},\tag{3}$$

$$\Xi_\sigma=\frac{\ell_0\sigma_0}{3g_\sigma^0}|\mathrm{Tr}\,\underline{\underline{\lambda}}_\sigma^V|,\quad \Xi_b=\frac{\ell_0\sigma_0}{3g_\sigma^0}|\mathrm{Tr}\,\underline{\underline{\lambda}}_b^V|,$$

where T_m is the melting temperature of the bulk and $s_T^{\sigma,b}$ is the Soret coefficient, which has the dimension of energy/K and is a rather difficult atomistic interpretation, especially in transition metals.[50,52] $\hat{Z}<0$ and $s_T\gtrless 0$ have opposite sign when compared with Al atoms. That means the thermomigration particle flux follows the direction of the heat flow, from the high-temperature region towards the low-temperature region. $\mathrm{Tr}\,\underline{\underline{\bar{\sigma}}}=\mathrm{Tr}\,\underline{\underline{\sigma}}/\sigma_0$ is the normalized trace of the local stress tensor, and σ_0 is one of the applied remote stress components (i.e., the applied uniaxial stress along the longitudinal direction) acting on the interconnect film. In the case of monovacancy mechanisms of diffusion, $\mathrm{Tr}\,\underline{\underline{\lambda}}_\sigma^V\lessgtr 0$

and $\mathrm{Tr}\,\underline{\underline{\lambda}}_b^V \leqslant 0$ are the traces of the elastic dipole tensors of the mobile monovacancy at the interfacial layer and in the bulk phase, respectively, which are both negative quantities and should not be confused with the activation volume of diffusion associated with the vacancy mechanism, which is a positive quantity. Therefore, for the drift diffusion operating with the monovacancy (or even for the self-interstitial) mechanisms the parameters defined above, $\Xi_{\sigma,b}$, are positive or negative quantities depending on the sign of the applied stress system and may be called the stress-field—elastic-dipole tensor interaction intensities for the interfacial layer and bulk solid phase, respectively. Since in general we have assumed that the traction is equal to zero for the free surfaces in the plain strain condition in 3D space, the trace may be given by $\mathrm{Tr}\,\underline{\underline{\bar{\sigma}}} \equiv (1+\upsilon)\bar{\sigma}_h$, where $\bar{\sigma}_h = \sigma_h/\sigma_0$ is identified as the normalized hoop stress. υ is Poisson's ratio. In these equations, E_0 denotes the electric field intensity directed along the specimen longitudinal axis. E is the usual Young modulus. $e|\hat{Z}|$ is the effective charge, which may be given in terms of atomic fractions x^i by $\hat{Z} = \Sigma_i x^i \hat{Z}^i$, for multicomponent alloys.

The various generalized mobilities are all normalized with respect to the mobility of the surface diffusion denoted by $\hat{M}_\sigma$. They are given, respectively, by

$$\hat{M}_\sigma = \frac{\tilde{D}_\sigma}{kT}\frac{h_\sigma}{\Omega_\sigma}, \quad \hat{M}_b = \frac{D_b^V N_b^V}{kT\Omega_b} \tag{4}$$

and

$$\bar{M}_{bv} = \frac{\hat{M}_{bv}\ell_0}{\hat{M}_\sigma}, \quad \bar{M}_b = \frac{\hat{M}_b \ell_0^2}{\hat{M}_\sigma}. \tag{5}$$

Here, $\bar{\Omega}_\sigma$ is the mean atomic volume of the chemical species in the surface layer of the solid phase. $\tilde{D}_\sigma$ is the isotropic part (i.e., the minimum value) of the surface diffusion coefficient. In the earlier description, we have tried to scale the time and space variables $\{t, \ell\}$ in the following fashion: first of all, $\hat{M}_\sigma$, an atomic mobility associated with mass flow at the surface layer, is defined by the relationship given in the previous paragraph, and then a new time scale is introduced by $\tau_0 = \ell_0^4/(\Omega_\sigma^2 \hat{M}_\sigma g_\sigma)$, where ℓ_0 is the arbitrary length scale and in the present paper the original thickness of the thin film is chosen as a natural scaling length: namely, $\ell_0 = h_0$.

In Eq. (1) the expression denoted by $\tilde{D}(\theta, \phi; m)$ is the angular part of the anisotropic surface diffusion, which may be represented by the following expression, assuming that D_0 is the minimum diffusivity or isotropic limiting value:

$$\tilde{D}(\theta, \phi; m) = D(\theta, \phi; m)/D_0 = \{1 + A\cos^2[m(\theta - \phi)]\}. \tag{6}$$

In the above relationships, $A \geqslant 0$ is the anisotropy constant and $n = 2m$ corresponds to the $2\pi/n$ degree of rotational folding associated with the zone axis of a given family of planes over which diffusion has taken place during the morphological evolution of surfaces of a thin single-crystal film. In the case of *sidewall morphological evolution*, the zone axis coincides with the initially undisturbed upper surface normal of the film; otherwise, it lies in the plane of the substrate along the some crystallographic directions of the single-crystal metallic interconnects.

A. Anisotropy in the surface Gibbs free energy and the cusp singularity

In Eq. (1), the expression denoted by $\bar{\bar{\gamma}}(\hat{\theta}, \hat{\phi}; m) \equiv \{\bar{\gamma}(\hat{\theta}, \hat{\phi}; m) + \bar{\gamma}_{\hat{\theta}\hat{\theta}}(\hat{\theta}, \hat{\phi}; m)\}$ is the angular part of the *surface stiffness*, given by $[\tilde{\gamma}(\hat{\theta}, \hat{\phi}; m)/\gamma^0]$. By following the general trend, one may introduce the trigonometric representation by defining the tilt angle $\hat{\phi}$ such that the surface normal of a selected vicinal plane coincides with the x axis when ϕ becomes equal to zero, $\hat{\phi} = 0$:

$$\bar{\gamma}(\hat{\theta}, \hat{\phi}; m) = \gamma(\hat{\theta}, \hat{\phi}; m)/\gamma_0 = \{1 + B\sin^2[m(\hat{\theta} - \hat{\phi})]\}, \tag{7}$$

where γ_0 is the minimum value of the surface Gibbs free energy density and $B \geqslant 0$ is the surface-specific Gibbs free energy *anisotropy constant* which is a positive quantity in the above *ad hoc* representation and measures the fractional degrees of roughness on the Wulff construction of the surface-specific Gibbs free energy. Using the above relationship denoted as Eq. (7) in connection with the calculation of $[\gamma_{\hat{\theta}\hat{\theta}} \leftarrow \partial^2\gamma/\partial\hat{\theta}^2]$, one may easily deduce the surface stiffness formula as

$$\tilde{\gamma}(\hat{\theta}, \hat{\phi}; m) = \gamma_0(1 + B/2)\left[1 - \frac{B(1-4m^2)}{B+2}\cos[2m(\hat{\theta} - \hat{\phi})]\right], \tag{8}$$

where $\hat{\theta} = [\pi/2 - \theta]$ is the angle between the line normal vector of the diffusion plane of a generalized cylindrical surface projected onto 2D space (surface normal in 3D) and the x axis of the global Cartesian reference system. In Fig. 1, the normalized surface-specific Gibbs free energy $\bar{\gamma}$ and the angular part of the surface stiffness $\bar{\bar{\gamma}} = (\gamma/\gamma^0)$ are illustrated in the polar plot for *sidewall planes* of a thin-film metallic single-crystal interconnect line, having a surface texture denoted by (001), where $n \equiv 2m = 4$.

According to Eq. (8), if the surface-specific Gibbs free energy anisotropy constant satisfies the inequality $B \leqslant 2/[|(1-4m^2)| - 1]$, then the surface stiffness can be positive definite, regardless of the orientation of the surface with respect to the EM direction. That means one should have the following set of upper limits for the anisotropy constants: $B \leqslant \{1, 1/7, 1/17\}$ in the case of twofold, fourfold, and sixfold symmetries, respectively. Otherwise, the system enters into the anomalous surface stiffness-induced instability regime. As can be seen from Fig. 1 for a given anisotropy constant $B = 0.2 > 1/7$ for the set of planes belonging to the [001] zone axis, imperfect faceting may occur at the cusp orientations (vicinal planes), because of the appreciable negative surface stiffness appearing in the directions $\langle 1^{\pm}10\rangle$, where one has concave topography (maxima in free energy profile). These negative surface stiffness spikes may cause inherent anomalous instability along those directions as will be discussed later in this paper. In general, the factional

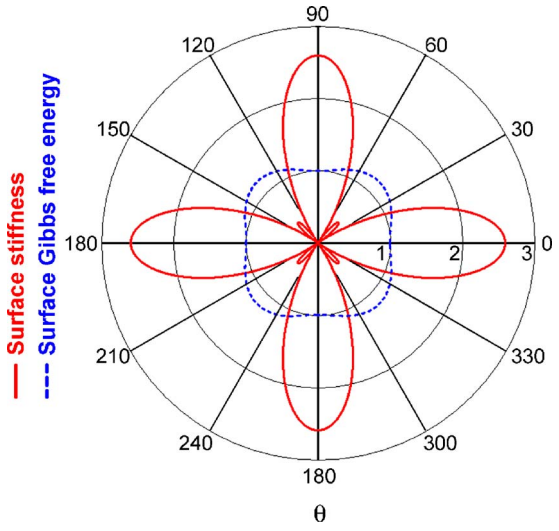

FIG. 1. (Color online) Typical behavior of the surface-specific Gibbs free energy and surface stiffness for a set of fourfold symmetry planes $\{01^{\mp}0\}$ and $\{1^{\pm}00\}$ in a fcc crystal having the [001] zone axis normal to the thin-film surface. The anisotropy constant $B=0.2$. The negative spikes of the surface stiffness for the sidewall drift diffusion are clearly seen along the $\langle 11^{\pm}0\rangle$ directions, which indicates inherent anomalous instability.

variations in the anisotropy constant are in the range of $|\delta B/B| \leqslant 0.20$ for the series of vicinal planes $\{111\}<\{110\}<\{100\}$ for most fcc and bcc metals and alloys.[53,54] Using the above expression, one may obtain the following normalized relationship, which enters directly into the growth rate formula, which is valid for the first-order perturbation theory, where one has $\{\theta|_{\varepsilon\to 0}\to 0\}$:

$$\bar{\hat{\gamma}}(\pi/2,\hat{\phi}) = (1+B/2)\left\{1+(-1)^{m+1}\frac{B(1-4m^2)}{B+2}\cos(2m\hat{\phi})\right\} \times(\text{surface stiffness}). \tag{9}$$

The representation of the surface Gibbs free energy by various trigonometric functions is very convenient for the discussion and analysis of its effects on the morphological evolution, as long as one does not deal with secondary fine features of the faceting and the equilibrium shapes of small crystals. Unfortunately, these cited features are very sensitive functions of the topography of the cusp regions in the construction of the surface-specific Gibbs free energy profile,[23] which is associated with the low-index crystal planes (singular or vicinal planes). According to the present findings one of the best analytical representative functions, which simulates the cusps on the Wulff topography, for numerical treatments may be achieved by mapping the *cycloid-curtate* curve around the unit circle in the polar coordinate system. The parametric representation of the curtate-cycloid curve[55] is given by the following set of equations after some modification or scaling procedures to suit our present physical objectives:

$$\gamma(\zeta) = \gamma_0\{1+\Psi\cos(\zeta)\}, \quad x(\zeta) = \{\zeta+\alpha\sin(\zeta)\}. \tag{10}$$

The parameter γ_0 is the mean value of the anisotropic surface-specific Gibbs free energy (density). Since the wavelength of the periodic extension of the above-modified curve is given by $\lambda=2\pi$, the basic range (the fundamental interval) of the variation of the rolling angle ς may be described by $[0,2n\pi]$. However, for the mapping procedure advocated in this paper a much better choice may be $[\pi,(2n+1)\pi]$, such that the surface normal of a selected vicinal (singular) plane coincides with the x axis when the tilt angle θ becomes equal to zero, $\hat{\phi}=0$, where $n=2m$ is the degree of folding associated with the rotation symmetry of the zone axis. The parameter denoted by $\Psi\equiv[\alpha/\gamma_0]$, which may be called the *Wulff surface roughness* (WSR) parameter, measures fractional variations of the surface Gibbs free energy with respect to the mean value and strictly corresponds to the anisotropy constant by definition. As we will show later in this section, it is a very important constant, which has an upper bond or a threshold value for a given α parameter, above which the capillary forces can no longer sustain or contribute to the stability of the surface disturbances. The corresponding parameter for Ψ in the trigonometric representation of the anisotropic surface Gibbs free energy is denoted by B, as defined previously. Above the threshold value of the WSR parameter, the surface stiffness takes negative values along certain sets (continuous) of directions in the Wulff construction. The parameter α describes topographic (shape) variations of the Wulff construction especially at the cusp regions in 2D space. When $\alpha=0$, the Wulff contour in the polar plot becomes a circle with a radius of γ_0, and when $\alpha=1$ (bifurcation between curtate and prolate cycloids), the contour forms periodic perfect cusps (the cracks) with periodicity of $2\pi/n$. Otherwise, in the range of $0<\alpha<1$, the contour is an undulating but smooth periodic curve, peaking between the cusps regions. The α parameter may be called the *Wulff surface topography* (WST) index; it will be clear very soon why it deserves that name. One may derive the following simple parametric relationship between a set of angles $\{\hat{\theta},\hat{\phi}\}$ defined previously and the surface stiffness and rolling angle ς using some legal calculus manipulations in connection with the definition of the surface stiffness, $\tilde{\gamma}=\gamma+\gamma_{\theta\theta}$. Hence, one writes, for the surface stiffness formula using the parametric representation in polar coordinates,

$$\hat{\gamma}(\zeta) = \gamma_0\left\{-n^2\Psi\frac{\alpha+\cos(\zeta)}{[1+\alpha\cos(\zeta)]^3}+\{1+\Psi\cos(\zeta)\}\right\},$$

$$x(\zeta) = n(\hat{\theta}-\hat{\phi}+\pi/n)\ \forall\ \pi\leqslant\zeta\leqslant(2n+1)\pi\ \forall\ 0\leqslant(\hat{\theta}-\phi) \leqslant 2\pi, \tag{11}$$

where the WST index $[0\leqslant\alpha<1]$ acts as a bifurcation adjustment or fine-tuning parameter for the cycloid, such that, at the upper limit, the transition from the curtate to the prolate cycloid curves takes place, which is accompanied by the formation of a Dirac δ distribution function singularity in the surface stiffness. The onset of the WSR parameter (WSR instability threshold), where the surface stiffness just enters into or touches the region of negative values in the Wulff polar diagram, is obtained for a given value of the WST index number from the detailed numerical analysis of Eq. (11). The WSR instability threshold level is plotted in Fig. 2

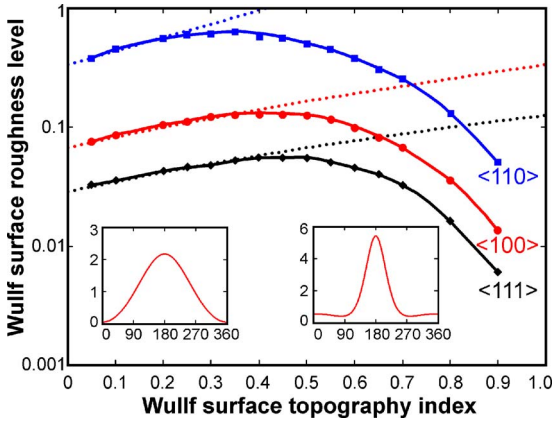

FIG. 2. (Color online) The instability threshold level of the *Wulff surface roughness parameter* (WSRP) is plotted with respect to the WST index number, which describes the form of the surface stiffness at the cusp regions, where a Dirac δ singularity enters into the scenario at $\alpha \rightarrow 1$.

as a function of the WST index number for various zone axes $\{n \subset 2,4,6\}$ in fcc crystalline solids.

In Fig. 2, there are two distinct sectors, where the *basic function* generating the Dirac δ distribution at the cusp regions shows completely different shapes: a smooth *Gaussian-like* form and a *sharp peak with dimples* at the shoulders, respectively. The first sector corresponds to the WST index numbers given by $(0 \leqslant \alpha \leqslant 0.35)$, where the minima in the surface stiffness profile irrevocably occur at $[\zeta_{\min}=2\pi,\ldots,2n\pi]$, and it is characterized by the Wulff surface contour having smooth Gaussian-like periodic undulations at the cusp regions.

These surface stiffness minima are also closely associated with the maxima of the surface Gibbs free energy profiles. Hence, in the lower-WST-index sector, the surface stiffness can be positive definite as long as one has the following inequality satisfied by the Wulff surface roughness parameter: $\Psi \leqslant \Psi^{crt} \equiv \{(1+\alpha)^2/[n^2-(1+\alpha)^2]\} \leqslant \{4/(n^2-4)\}_{\alpha \rightarrow 1}$, where Ψ^{crt} denotes the threshold level of the WSR parameter, above which the capillary-induced instabilities start to play a predominant role, which is also plotted as dashed lines for various fold numbers in this figure. Figure 2 clearly indicates that there is drastic decrease in the threshold level of the WSR parameter if one goes from the set of planes belonging to the $\langle 110 \rangle$ zone axis towards the sequence of sets of planes described by $\langle 100 \rangle$ and $\langle 111 \rangle$ zones.

The same figure also shows that with an increase in the WST index number, the threshold level of the WSRP shows first a linear increase in semilogarithmic scale and then suddenly turns at the knee points given by $\alpha_{\text{knee}} \cong 0.35$ towards the monotonically decreasing sector, where one has to impose much more severe instability requirements on the surface roughness parameter. This region corresponds to the upper-WST-index sector bounded by the interval $0.30 \leqslant \alpha \leqslant 1$, where the shape of the cusp on the Wulff construction becomes very important in the role played by the capillarity term in the instability, which cannot be deduced from the trigonometric representation of the Wulff surface topography, as will be illustrated later in this paper.

One may even give a tentative proof by some mathematical arguments, mostly adapted from the theory of generalized functions,[56] that the surface stiffness function $\bar{\tilde{\gamma}}(\varsigma)$ advocated in this paper, after the proper normalization and the interval setting, forms the *basic function* of the Dirac δ distribution function. In the upper-WST-index sector, where the minima occur at the shoulders of the surface stiffness profile in the cusp regions, the capillarity-induced instability—which may be called anomalous—becomes a great problem since one has a drastic decrease in the threshold level of the WSR parameter in that region as can be seen in Fig. 2. The real influence of this basic function, which is used in the representation of the surface stiffness, on the capillary-induced stability and faceting is still waiting to be explored by computer simulations. Another important advantage to using this basic function is that it can be easily adapted to the rounding effect of the temperature fluctuations on the surface-specific Gibbs free energy profile at the cusp regions by just playing with the WST index number as a function of temperature using some phenomenological relationship.

Typical polar plots of the surface Gibbs free energy and the surface stiffness are demonstrated in Fig. 3, for two different sectors in the WST-index-number range. Figure 3(a), which belongs to the lower-WST-index sector and is situated in the instability region, clearly shows that there is a factor of 2 improvements in the surface stiffness associated with quasicusp regions for the same anisotropy constants compared to Fig. 1, which is based on the trigonometric function. The instabilities along the $\langle 11^{\pm}0 \rangle$ directions do not change very much due to the high value of the WSR parameter above the threshold level compared to the mean surface Gibbs free energy.

In Fig. 3(b), the behavior of the surface stiffness profile is illustrated in the upper-WST-index sector, keeping the WSR parameter the same and above the threshold level, by zooming in on the polar origin, which clearly reveals the details of the subsidiary (negative) spikes arising from the dimples of the main peaks at the cusps. A close inspection also shows traces of $\langle 110 \rangle$ spikes (negative) with much less intensity.

B. Driving forces originated from the applied elastostatic field

There is great confusion in the literature, as discussed critically in our recent paper,[5] in appreciating the fundamental difference between the EDTI force and the fictitious chemical force implicitly associated with the gradient of the inhomogeneous ESED, since its individual identity in the thermodynamics sense can only be justified rigorously if the entropy density were independent of the stress field. Otherwise, it appears as a first-order approximation in the generalized Gibbs or Helmholtz free energy (with opposite sign) as a separate entity in conjunction with an additional term due to the *stress-field–latent-heat-tensor*[57] interaction given by $\bar{\bar{L}}^{b,0}_{\sigma,T} \otimes \bar{\bar{\sigma}}_b$ where the stress dependences are quadratic and linear, respectively. $\bar{\bar{L}}^{b,0}_{\sigma,T}$ is the latent-heat tensor referred to the unstrained state.[5]

For solid-to-solid interfacial reactions, one has to employ the following exact expression for the ESED contribution to the GFEDOT with the proper sign:

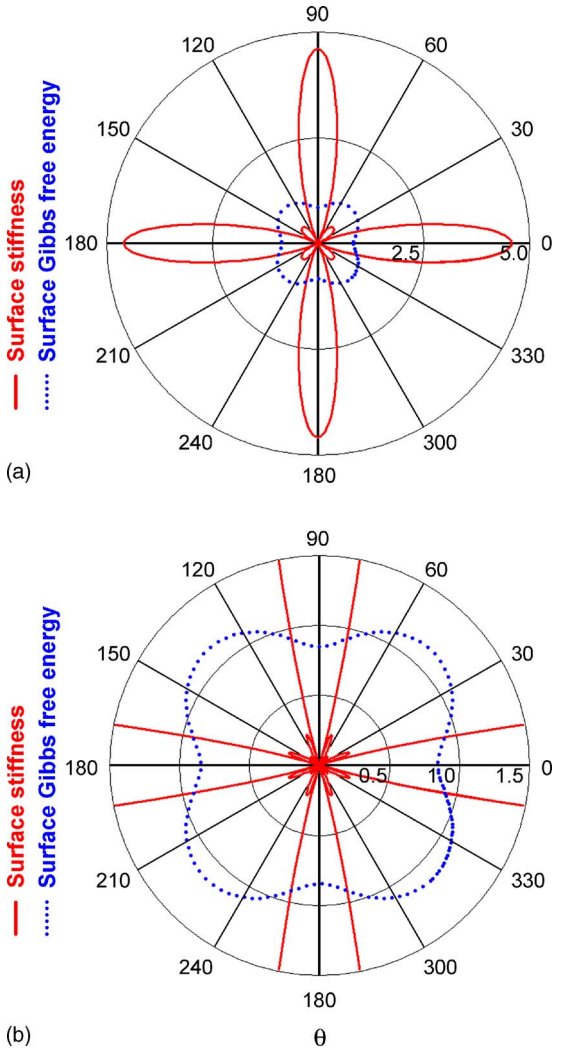

FIG. 3. (Color online) Typical behavior of the surface-specific Gibbs free energy and the surface stiffness illustrated in both WST index sectors by using the cycloid-curtate curve for the fourfold symmetry planes {100} having the [001] zone axis in a fcc crystal. The Wulff surface stiffness topography index (WST) is $\alpha=0.20$, and $\alpha=0.50$, respectively, and the surface roughness parameter is $\Psi=0.15$, which is above the threshold level for both regimes.

$$\Delta\bar{g}_{bv} = \Delta\bar{g}^{0}_{bv} - \frac{1}{2}\Delta_{bv}(\Omega\underline{\underline{\varepsilon}} \otimes \underline{\underline{\sigma}}) = \Delta\bar{g}^{0}_{bv} - \frac{1}{2}\Omega_{v}\underline{\sigma}_{v/\sigma} \cdot \underline{\underline{S}}_{v} \cdot \underline{\sigma}_{v/\sigma} + \frac{1}{2}\Omega_{b}\underline{\sigma}_{\sigma/b} \cdot \underline{\underline{S}}_{b} \cdot \underline{\sigma}_{\sigma/b}. \quad (12)$$

In the case of the crystalline silicon versus amorphous silicon transformation under the thermostatic stress (hydrostatic) system, where the traction-free boundary condition is no longer valid, the above expression should be considered in the driving force for the growth term as well as for the interface diffusion. In the above relationship, a pseudovector representation of the linear elasticity is used. $\underline{\underline{S}}_{v,b}$ are the isothermal (positive-definite) elastic stiffness (compliance) matrices, and $\Omega_{v,b}$ are the mean atomic volumes in the respective phases. $\Delta\bar{g}^{0}_{bv}$ represents the thermal part of the Gibbs free energy of the transformation of the flat interface. In the case of the fluid phase or even the amorphous solid phase, where shear stress relaxation may take place rather rapidly, the second term in the last expression of Eqs. (4) drops out completely, and one may have $\Delta\bar{g}_{bv} \simeq \Delta\bar{g}^{0}_{bv} + 1/2(\Omega_{b}\underline{\sigma}_{\sigma/b} \cdot \underline{\underline{S}}_{b} \cdot \underline{\sigma}_{\sigma/b} > 0$ (condensation or recrystallization). For a composite system made up of two different elastic solids separated by an interfacial layer, which has been also solved by Gao[59] using the 2D complex elasticity theory, one has to consider the stress-assisted bulk drift diffusion due to the EDTI in both phases. The above-cited relationship, in connection with Eq. (1), immediately shows that the strain energy density, regardless of the sign of the hoop stress at the surface layer, always prefers the condensation (i.e., recrystallization in the case of SPEG) process of flat surfaces and interfaces due to the growth term, just the opposite of the general claims.[22,30] Similarly, because of the high-strain-energy density localization at the trough regions compared to the crests, their displacement velocities will be much higher than the peaks, which causes a smoothing effect on the surface morphology. During the inverse reaction—namely, evaporation—just the opposite takes place: the displacement velocity of the crests will be faster than the trough, which also causes the surface modulations to smooth out. Therefore, regardless of the direction of the phase transformation, the elastic strain energy density has a positive effect on the surface under any applied stress system and for any modulation wavelength. Later in this section, one may anticipate that it also causes a healing effect on the surface roughness by the steady flow of matter from the crest (low-stress-concentration) regions towards the trough (high-stress-concentration) region due to its contribution to the surface drift diffusion term in Eq. (1), again regardless of the sign of the hoop stress. However, as will be discussed quantitatively in this work, the influence of the strain energy density on the overall stability and growth considerations of the surfaces and interfaces are almost negligible compared to the effects of the strain-field–elastic-dipole-tensor interactions up to extremely high stress levels: 21 GPa for silicon and 7.6 GPa and 15. GPa for aluminum and copper, respectively.

A close inspection of the contribution in Eq. (1) associated with the bulk diffusion, driven by the elastic dipole interaction caused by the applied elastostatic field, and knowledge of the elastic solution of the problem by Gao,[58,59] who has the most elegant, complete, and correct solution of the problem compared to Asaro and Tiller[22] and Srolovitz,[30] who have some problem in their 2D stress tensors, especially in the trace as well as in the deviatoric parts, but still can give the right answer for the hoop stress, one may observe later in this paper that the uniaxial tension smooths out the surface roughness by inhibiting the growth velocity of the crest regions and by simultaneously enhancing the displacement of the troughs by exactly the same factor, since the EDTI parameter $\Xi_{b} \geqslant 0$ is positive for the atomic hopping motion via the monovacancies in the case of uniaxial tension. The effect of the uniaxial compression appears to be just opposite in the case of bulk diffusion-assisted growth, where enhancement of the surface modulation or roughness is encouraged. This prediction is apparently in accordance with the observation of Aziz *et al.*,[60] who studied the motion

of the interface between crystalline and amorphous silicon (100) under the nonhydrostatic stress system. They have observed that the SPEG growth rate of the tensile side is greater than of the compressive side of elastically bent wafers and the interface roughness increases on the compressive side. However, this interpretation may be fictitious; namely, exactly the same conclusion could be reached by the stress dependence of the generalized growth mobility denoted by $M(\beta,\sigma_0;T)$ if the EDT associated with the mobile species at the saddle point configuration has negative trace but positive in-plain eigenvalues, as is the fact borne out by experiments, which will be elaborated later in this paper.

C. Stress dependence of the generalized growth mobility

Staying strictly in the domain of irreversible or classical thermodynamics, one cannot speculate very much on the generalized mobilities introduced by Onsager linear theory,[61,62] other than their symmetry properties. Therefore, one has to rely on either the atomistic models exposed to quantum statistical-mechanics treatments or some other heuristic quasithermokinetics arguments such as the transition-state theory, which is mostly used in the literature.[26,63] Utilizing the basic concepts of popular transition-state theory,[64] one may deduce the generalized mobility from the gross reaction rate constant by considering not only the forward but also the backward reactions, which are closely connected with the mesoscopic structure of the interfacial layer, during the phase transformation. While elaborating this heuristic treatment in the context of the enlarged transition-state theory, the Gibbs free energy of the activated complex subsystem must be also supplemented by the elastic dipole interaction energy of the mobile atomic species at the saddle point configuration, as a part of the internal energy of activation, u^*. This contribution arises by the mutual interaction between the externally applied stress system and the induced strain field generated by the temporal occupation of the saddle point configuration by the activated atomic species in the interfacial layer. Keeping this statement in mind, one can easily calculate the following universal formula for the gross reaction rate constant $\mathfrak{R}_{v\Rightarrow b}$ for the transformation, symbolically represented by $v\Rightarrow b$ (i.e., recrystallization of amorphous Si into the crystalline state or vice versa) with a little arithmetic manipulations of terms:

$$\mathfrak{R}_{v\Rightarrow b} = 2\mathfrak{R}_0 \exp\left\{-\frac{[\hat{g}^*_\sigma - (\hat{g}_b+\hat{g}_v)/2]}{kT}\right\}\sinh[-\Delta\hat{g}_{vb}/2kT]$$
$$\cong \mathfrak{R}_0 \exp\left\{-\frac{[\hat{g}^*_\sigma - (\hat{g}_b+\hat{g}_v)/2]}{kT}\right\}[(\hat{g}_v-\hat{g}_b)/kT]$$
$$\times(\forall T\approx T_{trans}),$$
$$\cong \mathfrak{R}_0 \exp\left\{-\frac{[\Delta\hat{g}^*_{vb}]}{kT}\right\}\exp[-\Delta\hat{g}_{vb}/kT] \quad (\forall T<T_{trans}), \tag{13}$$

where $\mathfrak{R}_0=\varsigma(\beta)kT/h$ is the attempt frequency and numerically it is about equal to the Debye vibration frequency [$\approx 10^{12}$ s^{-1}]. Here $\varsigma(\beta)=\exp[\Delta S^*_\sigma(\beta)/k]$ is the steric factor, as explained previously. $\Delta\hat{g}^*_{vb}$ and $\Delta\hat{g}_{vb}=\hat{g}_b-\hat{g}_v<0$ are the Gibbs free energy of the activation and the Gibbs free energy of the transformation denoted symbolically as $v\Rightarrow b$, respectively. $\Delta\hat{g}^*_{vb}$ is referred to as the mean Gibbs free energy associated with both phases $[\Delta\hat{g}^*_{vb}\equiv\hat{g}^*_\sigma-(\hat{g}_b+\hat{g}_v)/2]$ and evaluated just at the adjacent regions of both sides of the interfacial layer. The cap sign over the various generalized Gibbs free energies indicates (i.e., $\hat{g}\cong[\hat{u}_{th}-T\hat{s}_{th}-\hat{w}]$) that this quantity is referred to the particle representation. The unabridged form of the above kinetics equation has been adapted by many authors empirically, including Liang and Suo[46] and Barvosa-Carter and Aziz,[43] in their formulations. While writing the second and third lines in Eq. (13), using the properties of the sinh(·) function, it has been presumed that the phase denoted by b is a stable phase below the transformation temperature: namely, $\Delta\hat{g}_{vb}<0$. T_{trans} denotes the transformation temperature (or some type of softening or roughening temperature) at which the Gibbs free energy of the reaction becomes identically equal to zero. This hypothetical transformation *proxy mimics* the recrystallization of amorphous Si (supercooled liquid state) into crystalline Si below the quasitransition temperature. The last term between the brackets, which appears in the linearized second line in the above set of equations, corresponds to the generalized transverse driving force per particle (condensation or recrystallization) acting on the flat interface, and its positive value $F_{vb}\equiv-\Delta\hat{g}_{vb}/T=(\hat{g}_v-\hat{g}_b)/T>0$ indicates that condensation or recrystallization take place as a natural process. This term is a special case of our generalized thermodynamic force obtained for the curved interfaces by the irreversible thermodynamic treatment of the global entropy production,[4] and the cofactor of the driving force simply corresponds to the generalized mobility, M_{vb}/k in our growth term in Eq. (1). Hence, one may write immediately, by the principle of correspondence, the following expression for the generalized mobility by rearranging the stress-dependent terms properly in the Gibbs free energies and using the fact that an activated complex interacts with the stress field through the EDTI term:

$$\hat{M}_{vb}(\sigma,\beta;T)\overset{def}{\equiv}\frac{M_{vb}}{kT}=\frac{\mathfrak{R}_0}{kT}e^{-\Delta\hat{g}^*_{vb}/kT}=\frac{\mathfrak{R}_0}{kT}e^{\Omega\Delta s^*_{th}/k}\exp\left\{-\frac{\Omega[\Delta u^*_{th}-w^*-\underline{\underline{\lambda}}^*\otimes\underline{\underline{\sigma}}+(w_b+w_v)/2]}{kT}\right\}=\frac{\mathfrak{R}_0}{kT}e^{\Omega\Delta s^*_{th}/k}$$
$$\times\exp\left\{-\frac{\Omega[\Delta u^*_{th}-\underline{\underline{\lambda}}^*\otimes\underline{\underline{\sigma}}]}{kT}\right\}\equiv\hat{M}^0_{vb}(\beta;T)\exp\left(\frac{\Omega\underline{\underline{\lambda}}^*\otimes\underline{\underline{\sigma}}}{kT}\right), \tag{14}$$

where $\Delta\hat{u}^*_{th} \equiv \hat{u}^*_{th} - (\hat{u}^b_{th} + \hat{u}^v_{th})/2$ is the thermal part of the activation energy referred to as the mean energy of the adjacent bulk phases, separated by the interfacial layer, and the subscript *th* denotes the stress-independent parts of the characteristic functions (thermal component) assuming that the entropy is stress independent. $\hat{M}^0_{vb}(\beta;T)$ is the generalized mobility in the absence of the external stress system, which may be depend on the orientation of the interface (anisotropy) due to the steric factor denoted by $e^{\Omega\Delta s^*_{th}/k}$. In writing the above equations, one should recall that the elastic dipole interaction energy associated with the activated complex atom, as a temporal point defect at the saddle point configuration in the interfacial layer, is given by $u^*_{EDT} = -\Omega_\sigma \underline{\underline{\lambda}}^*_\sigma \otimes \underline{\underline{\varrho}}_\sigma$. In general, the elastic dipole tensor at the saddle point configuration $\underline{\underline{\lambda}}^*$ is axisymmetric (but not necessarily universally true) and its eigenvalues may depend upon the orientation of the interfacial layer in crystalline solids similar to the interfacial tension tensor as demonstrated recently by Ogurtani and Oren.[5] From the definition of the macroscopic stress and strain tensors in an elastic continuum and the adapted reference system for the thermodynamic functions for the activated complex, one has $[w^* = (w_b + w_v)/2]$. Similarly, the driving force for the flat interfacial reaction in terms of volumetric densities may be written as

$$F_{vb} = -\frac{\Omega}{T}[(g_b - g_v)] = -\frac{\Omega}{T}[\Delta g^0_{vb} + w_v - w_b]. \quad (15)$$

The corresponding interface displacement velocity v_d due to the phase transformation at the curved interfacial layer may be written as in the real-time and -space domain,

$$\mathrm{v}_d = -\hat{M}_{bv}(\beta,\sigma;T)\Omega^2_b[\Delta g^0_{bv} - w_v + w_b + g_\sigma\kappa]. \quad (16)$$

In the case of fluids or the amorphous solid phase where the stress relaxation takes place rather easily (i.e., excluding the *hydrostatic stresses*) one may assume that $w_v \cong 0$. Therefore, the positive-definite strain energy density of the bulk phase $w_b \geqslant 0$ adjacent to the interfacial layer always enhances the condensation process or stabilizes the stress-carrying solid bulk phase. One may write the following expression for the generalized volumetric Gibbs free energy density by splitting the internal energy into three parts: namely, thermal energy, strain energy, and elastic dipole tensor interaction energy, assuming that the entropy is independent of the applied stress system $s^* \cong s^*_{th}$ or is a first-order approximation, the latent-heat-tensor contribution being negligible, where the thermal components of the thermodynamic characteristic functions refer to their volumetric densities. Hence, one writes[13]

$$g^* = u^* - Ts^* - \underline{\underline{\varepsilon}}^* \otimes \underline{\underline{\varrho}}^* = \left[u^*_{th} + u^*_{EDTI} + \frac{1}{2}\underline{\underline{\varepsilon}}^* \otimes \underline{\underline{\varrho}}^*\right] - Ts^*$$

$$- \underline{\underline{\varepsilon}}^* \otimes \underline{\underline{\varrho}}^* \cong [u^*_{th} - Ts^*_{th}] - \underline{\underline{\lambda}}^*_\sigma \otimes \underline{\underline{\varrho}}^* - \frac{1}{2}\underline{\underline{\varepsilon}}^* \otimes \underline{\underline{\varrho}}^*$$

$$\equiv f^*_{th} - \underline{\underline{\lambda}}^*_\sigma \otimes \underline{\underline{\varrho}}^* - w^*, \quad (17)$$

where one has the elastic strain energy density given by $w^* = \underline{\underline{\varepsilon}}^* \otimes \underline{\underline{\varrho}}^*/2$ and the elastic dipole tensor for the activated complex state is denoted by $\underline{\underline{\lambda}}^*_\sigma$, which is the intrinsic property of the system at the saddle point configuration, which may have tetragonal symmetry, similar to the interfacial tension tensor in the interfacial layer. f^*_{th} and u^*_{th} are the thermal parts of the Helmholtz and internal energy densities, respectively. Similarly s^*_{th} represents thermal part of the entropy density.

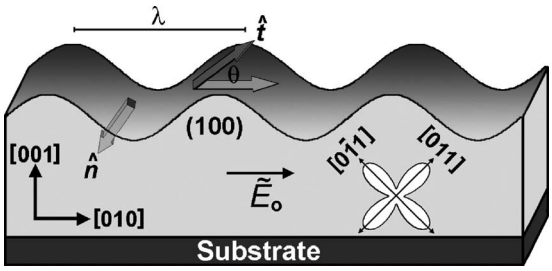

FIG. 4. Side view of a metallic single-crystal thin film, with a preexistent sinusoidal wave on the surface just before the onset of the application of the electric field. This configuration corresponds to the fourfold degrees of rotation symmetry, $n=4$, and the tilt angle $\phi=45°$ as far as the diffusion and the surface-specific Gibbs free energy dyadics are concerned.

III. UNIFIED LINEAR INSTABILITY ANALYSIS

In this section a concise treatment of the linear first-order stability analysis of the governing equation (1) is presented, where the traveling plane wave, propagating on the surface of a thin single-crystal film (infinite extent), with complex argument is employed as the initial data. The two last terms in Eq. (1), which are discussed in detail by Ogurtani and Oren[5,13] in the formulation of the local and global entropy production associated with interfacial layer displacement, can be used for the general phase transformation between two condensed phases. Similarly, the growth displacement velocity expression for a spherical second-phase particle in a bulk matrix can be easily deduced as a special case of our general formulation by introducing the concept of the critical radius as $r_c = \kappa^{-1} = -\gamma_\sigma/\Delta g_{bv}$, which reduces to the well-known Hillert[65] theory, which in its original derivation makes use of the Lifshitz-Slyyozov-Wagner (LSW) theory of interface-controlled particle coarsening in the absence of the stress field.[30]

A. Effect of electromigration on the instability of single-crystal thin films

The morphology of an initially perfectly flat (001) surface having a perturbation in the shape of a sinusoidal wave is demonstrated in Fig. 4, where the positive direction of the electric field is from the left (anode) to the right (cathode) [010]. The scaled interconnect thickness is denoted as $\bar{h}_0 = 1$, and the wave vector and the wavelength are given by $\bar{k} = kh_0$ and $\bar{\lambda} = \lambda/h_0$, respectively. These are all scaled with respect to the arbitrary length chosen as $\ell_0 = h_0$ for convenience in this paper. Here h_0 is the initial uniform thickness of the metallic thin-film interconnect before it is exposed to any surface disturbances.

In this subsection the combined effects of capillary migration and electromigration on the instability on the anisotropic solid surfaces are considered. One can easily show that the normalized and scaled equation (1), in the Cartesian coordinate system for a solid bulk matrix-fluid phase interface, takes the following exact form using the conventional definition of the curvature of 2D curves. One should recall that in Eq. (1), the positive direction of the surface displacement velocity is chosen towards the bulk phase and the curvature term is so defined that the surface bulge or crest has a negative sign $\kappa<0$, where we have taken the realistic void phase as a reference system in our original formulation:

$$-f(h_x)h_t = f(h_x)\partial_x\{D(\cdot)f(h_x)\partial_x[\Delta\bar{g}_{bv} + \chi\vartheta + \bar{\Xi}_s\sigma_h - \Upsilon_\sigma\bar{T}_\sigma + \bar{\tilde{\gamma}}(\cdot)f^3(h_x)h_{xx}]\} + \bar{M}_{bv}[\Delta\bar{g}_{bv} + \bar{\tilde{\gamma}}(\cdot)f^3(h_x)h_{xx}] + \bar{M}_b\bar{\Xi}_b f(h_x)\hat{n}\cdot\bar{\nabla}_2(\mathrm{Tr}\,\bar{\underline{g}}_{b/s}) - \bar{M}_b\Upsilon_b\hat{n}\cdot\bar{\nabla}_2(\bar{T}_{b/s}). \tag{18}$$

Here, one should make it clear that the growth parts of this master equation, which are situated in the second line of the above expression, are also rigorously valid for the interfacial later between two condensed phases, but not the surface drift-diffusion part that appears in the first line, in the physical context of the original formulation,[5] without putting some extra constrain on the composite system, where EDTI parameter is redefined in the plain-strain condition as $\bar{\Xi}_s=(1+\upsilon)\frac{\ell_0\sigma_0}{3g_s^0}|\mathrm{Tr}\,\underline{\lambda}|_s$, which is more convenient for the surfaces free of traction.

We should mentioned here that all those quantities appearing in the present treatment are normalized and scaled quantities. In order to simplify the notation we do not use an overbar over the scaled space and time variables, and the kinematics parameters such wave numbers k, phase velocities υ, the surface profile function h, and the decay rate Γ [i.e., $x\leftarrow\bar{x}\equiv x/h_0$, $t\leftarrow\bar{t}\equiv t/\tau$, $h\leftarrow\bar{h}(x,t)=h(x,t)/h_0$], where h is a shorthand notation for the time- and space-dependent and normalized disturbed surface profile having infinite extent $[-\infty,+\infty]$, and $f(h_x)$ is called the structure function, which is given by

$$f(h_x) = (1+h_x^2)^{-1/2}. \tag{19}$$

One may also recall the following transformations, which are used in the derivation of the master equation (18):

$$\partial_x \equiv (1+h_x^2)^{-1}h_{xx}\partial_\theta, \quad \partial_\ell \equiv (1+h_x^2)^{-1/2}\partial_x. \tag{20}$$

The quasielectrostatic potential φ satisfies the Laplace equation $\nabla^2\phi=0$ in 2D space and the Neumann boundary conditions at the inactive and active surfaces, respectively:

$$\varphi_y(0,x;t)=0, \quad \varphi_y(h,x;t)=h_x(x,t)\varphi_x(h,x;t). \tag{21}$$

As justified in due time, in the linear stability analysis of the governing equation, the initial data may be supplied by the following expression for the interface profile, which shows a traveling plane-wave perturbation having complex arguments and superimposed on a constant velocity displacement of a flat interface (i.e., evaporation and condensation):

$$h = 1 + \bar{M}_{vb}\Delta\bar{g}_{bv}t + \varepsilon a_\varepsilon\{\exp[ik(x-\mathrm{v}t)] + \mathrm{c.c.}\}, \tag{22}$$

where a_ε, the amplitude of the traveling wave, is $k\leftarrow 2\pi/\bar{\lambda}=kh_0$, which is the normalized wave number, and $0\leqslant\varepsilon\leqslant 1$ is the perturbation order operator. v is a complex number (i.e., phase velocity), which carries the most important information concerning the dynamical behavior of the system. In a certain treatment, one uses $\omega=k\mathrm{v}$, which is called the frequency index, which is very convenient to define the group velocity: namely, $\mathrm{v}_g=\partial\omega/\partial k$. The real part of the complex velocity, v_R, corresponds to the phase velocity (dispersion), and the imaginary part, v_{Im}, deals with the dissipation or growth rate $\Gamma=k\mathrm{v}_{\mathrm{Im}}$. Similarly, the normalized quasielectrostatic potential at the active sidewall (or upper surface) may be represented by the following expression, which was first presented by Schimschak and Krug[10] and later further elaborated by Brush and Oren [66]:

$$\bar{\varphi}(x,y;t) = -x - i\varepsilon a_\varepsilon\frac{\cosh(ky)}{\sinh(k)}\exp[ik(x-\mathrm{v}t)] + \mathrm{c.c.}, \tag{23}$$

and for the upper normalized active surface ($y=1$) one writes

$$\bar{\varphi}(x,t) = -x - i\varepsilon a_\varepsilon\coth(k)\exp[ik(x-\mathrm{v}t)] + \mathrm{c.c.} \cong -x - i\varepsilon a_\varepsilon\frac{1+k}{k}\exp[ik(x-\mathrm{v}t)] + \mathrm{c.c.} \tag{24}$$

In the above expression, we have introduced the following very accurate approximation for the cofactor given by $\coth(k)\cong(1+k)/k$ in the amplitude of the electrostatic field induced by the surface undulations. This cofactor may be called the *film thickness enhancement* (FTE) parameter, which becomes very important in the dispersion relationship associated with the propagation velocities of the EM-driven surface disturbances, especially at the long-wave limit as described by $\{k\leqslant 1\Rightarrow\lambda\geqslant 2\pi h_0\}$. The relationship (23) also shows clearly that the influence of the surface disturbance on the electrostatic potential decay is almost exponential with the distance from the initially flat surface position $y=1$. However, the disturbance-affected zone is scaled down by the critical wavelength given by $\lambda_{crt}=2\pi h_0$ in real space.

It can be easily anticipated that for the first-order perturbation represented by the $\varepsilon\Rightarrow 1$ operator, the governing equation (1) takes the following concise form without making any additional assumptions about the structure function, which virtually reduces to unity:

$$h_t = \lim_{\theta\to 0}\{-\chi[D(\theta,\phi)\partial_{xx} + \partial_x D(\theta,\phi)\partial_x^C]\bar{\vartheta} - D(\theta,\phi)\bar{\gamma}(\pi/2-\theta,\phi)h_{xxxx} - [D(\theta,\phi)\partial_{xx} + \partial_x D(\theta,\phi)\partial_x^C]\times[\Delta\bar{g}_{bv} + \bar{\Xi}_s\bar{\sigma}_h - \Upsilon_\sigma\bar{T}_\sigma] + \bar{M}_{vb}[\Delta\bar{g}_{bv} + \bar{\gamma}(\pi/2-\theta,\phi)h_{xx}] - \bar{M}_b\bar{\Xi}_b\hat{n}\cdot\bar{\nabla}_2(\mathrm{Tr}\,\bar{\underline{g}}_{b/\sigma}) + \bar{M}_b\Upsilon_b\hat{n}\cdot\bar{\nabla}_2(\bar{T}_{b/s})\}. \tag{25}$$

In the above relationship the superscript over the partial differential (PD) operator ∂_x^C implies the extraction of the constant term from the gradient of the operand function. This operator is intentionally introduced and kept here in order to

treat those problems where there is a (constant) strain field gradient along the specimen longitudinal axis induced by the steady-state heat flow and/or by the electromigration (Blesh effect). In the case of homogenous fields, this term drops out automatically. The elastic strain energy density of the solid phase, like other intensive quantities, is evaluated just beneath the surface layer. In addition, if one assumes that the thermal part of the Gibbs free energy of the transformation $\Delta\bar{g}^0_{bv}$ is homogeneous along the surface layer and the transformation mobility $\bar{M}^0_{vb}$ is independent of the applied stress and orientation of the surface, then one may write

$$ik\mathrm{v} - \bar{M}^0_{vb}(\Delta\bar{g}^0_{bv} + \bar{w}^0_b) = i\chi k^2 \coth(kh_0)[1 + A\cos^2 m\phi] + \chi mk^2 A \sin[2m\phi] + [1 + A\cos^2 m\phi][\hat{\gamma}(\pi/2,\phi)k^4] + \{[1 + A\cos^2 m\phi]\partial_{xx} + mA\sin[2m\phi]\partial^C_x\}[\Xi_s\bar{\sigma}_h + \Sigma\bar{\sigma}^2_h - \Upsilon_\sigma\bar{T}_\sigma] - \bar{M}^0_{vb}(\Delta\bar{g}^0_{bv} + \bar{w}^0_b) + \bar{M}^0_{vb}\{\hat{\gamma}(\pi/2,\phi)k^2 - \Sigma\bar{\sigma}^2_h\} + \bar{M}_b\Xi_b\hat{n}\cdot\bar{\nabla}_2(\mathrm{Tr}\,\bar{\bar{\sigma}}_{b/\sigma}) - \bar{M}_b\Upsilon_b\hat{n}\cdot\bar{\nabla}_2(\bar{T}_{b/s}). \quad (26)$$

In our future discussions the thermomigration terms appearing in the above expression will not be reproduced, excluding the discussion section, since we have no analytical information concerning the temperature distribution associated with the heat generated by the Joule effect and/or the possible phase transformation associated with the condensation or recrystallization processes taking place during displacement of the interfacial layer. However, one may easily speculate that for the undercooled system, the mean temperature at the trough region is kept higher than the crest region by the heat which has evolved during the condensation. That means there will be steady thermomigration of atomic species from the trough region towards the crest opposing the temperature gradient and invoking the interface roughness.

In Eq. (26), $\Sigma\bar{\sigma}^2_h$ represents the first-order contribution to the ESED due to the formation of surface undulations on the surfaces, otherwise flat and traction free. $\bar{w}^0_b$ is the elastic strain energy density for the flat surface. The above general relationship in the absence of an external applied stress field yields the following expressions, for the growth rate and the phase velocity, by separating the real and imaginary parts of the complex velocity such as $\mathrm{v}=\mathrm{v}_R+i\mathrm{v}_{\mathrm{Im}}$, where the real part corresponds to the propagation or phase velocity and the imaginary part is related to the *growth rate constant* denoted by Γ. Then one may have the following connections by equating the real and imaginary parts of both sides of the above equation:

$$\mathrm{v}_R = \chi k \coth(k)[1 + A\cos^2 m\phi]. \quad (27)$$

The above expression takes the following form after the renormalization procedure in the real-time and -space domain:

$$V(k) = \frac{\tilde{D}_\sigma h_\sigma e|Z_\sigma|\rho_b J_b}{kT} k\coth(kh_0)[1 + A\cos^2 m\phi]$$

$$\cong \frac{\tilde{D}_\sigma h_\sigma e|Z_\sigma|\rho_b J_b}{kT} k[1 + A\cos^2 m\phi] \quad (\forall\ kh_0 \geqslant 2)$$

$$\cong \frac{\tilde{D}_\sigma h_\sigma e|Z_\sigma|\rho_b J_b}{kTh_0}(1 + 0.25(kh_0)^2)$$

$$\times[1 + A\cos^2 m\phi] \quad (\forall\ kh_0 < 2). \quad (28)$$

The last two very accurate approximations are added in order to show the dispersion relationships for the short- and long-wavelength sectors, respectively. The second line clearly reveals that the dispersion relationship is linear and does not depend on the film thickness in the short-wavelength sector, $kh_0 \geqslant 2$. On the other hand, the third line indicates that in the long-wavelength sector the velocity dispersion relationship is quadratic and the limiting value is inversely proportional to the film thickness. Equation (28) shows that the disturbance propagation velocity is always from the anode site to the cathode site in the direction of the applied electric field.

The disturbance growth rate associated with electromigration and capillarity effects may be easily deduced from Eq. (26), which results in

$$\Gamma \equiv k\mathrm{v}_{\mathrm{Im}} = -\chi mk^2 A\sin[2m\phi] - \{[1 + A\cos^2 m\phi]k^2 + \bar{M}^0_{vb}\}\hat{\gamma}(\pi/2,\hat{\phi})k^2. \quad (29)$$

In Fig. 5, the growth rate for a set of planes belonging to the zone axis $\langle 110\rangle$ having twofold rotational symmetry is presented in a 3D plot as a function of tilt angle and wave number assuming that the electron wind intensity is given by ($\chi=0.75$) and the diffusion anisotropy constant has a reasonable value of $A=5$, where two different surface stiffness regimes are illustrated. In the first case, the surface stiffness is positive definite at any direction in the Wulff construction, and in the second case the surface stiffness shows negative values along certain well-defined orientations as described previously. In order to illustrate the behavior of the growth rate constant for the first case, two extreme values of surface stiffness anisotropy parameter, $B=0$ and $B=1$, are employed, respectively. It is clearly seen from these figures cited as (a) and (b) that the instability region in the case of positive-definite surface stiffness, which is described by the projection at the $\Gamma=0$ plane, is singly connected to closed domains that cover tilt angles in an open interval of $\pi/2<\phi<\pi$ and some small-wave-number regions having a lower bound $k=0\Rightarrow(\lambda\to\infty)$. The immediate effect of the surface stiffness anisotropy on the growth rate may be easily observed if one

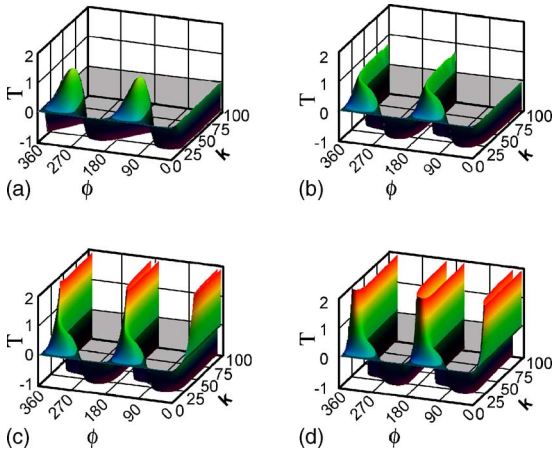

FIG. 5. (Color online) The growth rate constants of sinusoidal surface disturbances under capillary and EM forces are plotted with respect to the tilt angle (0-2π) and the wave number (0-π) for a twofold symmetry zone axis ⟨110⟩ for the two different regimes associated with the surface stiffness: the normal instability regime where the surface stiffness is positive ($B=0$, isotropic; $B=1.0$, full anisotropy) and the anomalous instability regime showing negative values along some directions described by ($B=1.1, 2.0$). The diffusion anisotropy constant $A=5$, the applied EW intensity $\chi=0.75$.

compares Fig. 5(b) with Fig. 5(a), which corresponds to the isotropic case. The surface stiffness anisotropy, according to Fig. 5(b), pushes the instability domain towards high tilt angles ($\phi \rightarrow \pi/m$) in the fundamental interval and drastically extends the upper bound of the wave numbers into the short-wavelength region. Hence, the most critical configuration, as far as the onset of the instability regime is concerned, occurs when the orientation of the principal axis of the surface stiffness dyadic lies almost parallel but opposite in direction to the applied electric field, which is assumed to be lying on the surface of the thin-film interconnect.

The effects of the surface stiffness in the negative value regime on the growth rate (instability) may be easily seen in Figs. 5(c) and 5(d), where $B=1.1$ and $B=2$ are used for demonstrations, respectively. Namely, the instability domain starts to extend towards the forbidden tilt angle ranges for the twofold rotational symmetry, which are denoted by $(0, \pi/2)$ and its periodic extension given by $(\pi, 3\pi/2)$. Normally these ranges correspond to the capillarity-dominating regime, where one has the dissipative mode in operation under applied EM forces, which smooths out any surface disturbances regardless of its wavelength. The application of the renormalization procedure to expression (29) similarly yields the following relationship in real space, where Γ may be called the disturbance growth rate (DGR) constant and its positive value represents instability of the surface morphological evolutions:

$$\Gamma = -\frac{D_\sigma h_\sigma k^2}{kT}\{Ae\hat{Z}\rho_b J_b m \sin(2m\phi) + \Omega_\sigma g_\sigma^0 k^2[1 + A\cos^2(m\phi)]\bar{\bar{\gamma}}(\pi/2, \hat{\phi}; B)\} - \hat{M}_{vb}^0 \Omega_\sigma^2 g_\sigma^0 \bar{\bar{\gamma}}(\pi/2, \hat{\phi}; B)k^2. \quad (30)$$

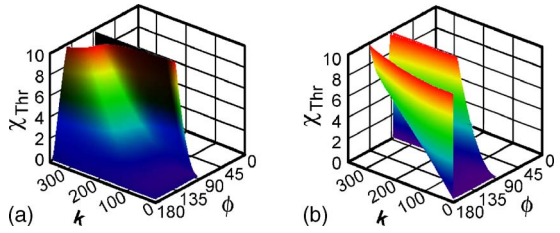

FIG. 6. (Color online) The instability boundary surfaces for the extremely anisotropic ($B=1$) and the isotropic ($B=0$) cases are plotted in (a) and (b), respectively, in terms of the electron wind intensity threshold level, wave vector, and tilt angle for the twofold symmetry zone axis ⟨110⟩. $A=5$ and $M_{vb}=0$. In these figures, there are singularities at $\phi=[\pi/2m, \pi/m]$, where the EW intensity ($\chi \rightarrow \infty$) cannot be defined by formula (32).

The relaxation time of the dynamical system may be obtained from a simple connection such as $\tau_R=-1/\Gamma$. The instability is closely connected to the applied electric field and the tilt angle. The range $\pi/2m < \phi < \pi/m$ corresponds to the possible (normal) instability growth region even in the absence of the surface Gibbs free energy anisotropy. Similarly, the surface tension and the ESED contributions are preferred for stability unless the surface stiffness $\bar{\bar{\gamma}}(\pi/2, \phi)$ becomes a negative value, which may cause a dramatic instability problem as will be discussed in this section in connection with vicinal (singular) planes.

Similarly, by utilizing Eq. (29), one may study the boundary surface in 3D space described by $[\chi, k, \phi]$, which separates the instability domain from the stability region, for a given set of system parameters: namely, the anisotropy constants $[A, B]$, the fold number $[m]$, and the generalized phase transformation (growth) mobility denoted as $\bar{M}_{vb}$. Hence, one may write the following expression to define the *instability boundary surface* in terms of the threshold or the instability onset value of the EW intensity parameter $\chi_{thr}(k, \phi)$ under a given set of system parameters as a function of wave number and tilt angle, assuming that the surface diffusion and the surface-specific Gibbs free energy dyadics have a similar orientation (not necessarily true universally):

$$\chi_{thr}(k, \phi) = -\frac{\bar{\bar{\gamma}}(\pi/2, \varphi; B)}{\{mA \sin[2m\phi]\}}\{[1 + A\cos^2 m\phi]k^2 + M_{vb}\}, \quad (31)$$

$$\forall\, \phi \neq \left\{\frac{\pi}{2m}, \frac{\pi}{m}\right\}.$$

In Fig. 6, the *threshold level* of the EW intensity as a function of tilt angle and normalized wave number is presented as a 3D plot for the set of planes having a twofold symmetry zone axis ⟨110⟩ in fcc structure, where the surface diffusion anisotropy constant is taken as $A=5$ and the surface stiffness anisotropy constant is assumed to have two extreme values: namely, $B=0$ (isotropic) and $B=1$ (upper bond for the surface stiffness stability). In these figures instability domains, which are bounded by either the combination of threshold surface (χ, ϕ) and $(\chi, k=\pi/m)$ planes or the threshold sur-

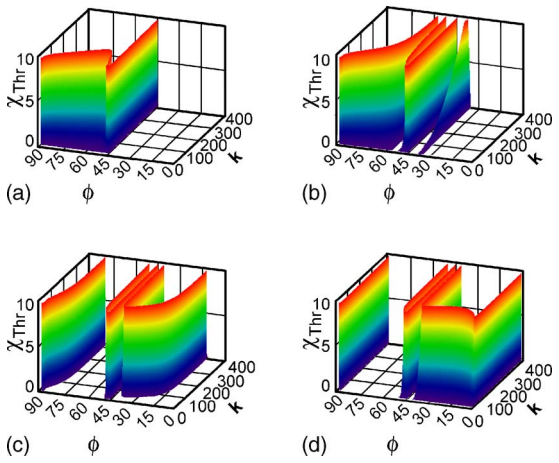

FIG. 7. (Color online) The instability boundary surfaces associated with various surface stiffness anisotropy constants below ($\Psi=0.03$) and above ($\Psi=0.08,0.20,0.30$) the capillarity threshold level is illustrated for a fourfold symmetry zone axis ⟨100⟩, respectively. The anomalous instability, which occupies the forbidden tilt angle interval, is clearly demonstrated in these figures, where $A=5$, $M_{vb}=0$, and $\alpha=0.70$.

face and (χ,ϕ) plane, respectively, can be easily distinguished from the stability region.

The growth rate constant relationship (29) in the absence of an applied stress field shows very clearly that if the surface stiffness that is described by the trigonometric function satisfies an inequality given by $B_{2m}\leqslant 2[|1-4m^2|-1]^{-1}$, which may be represented quantitatively by $\{B_2<1, B_3<1/7, B_6<1/17\}$ for various fold numbers, then the capillary force represented by the second term prefers absolute stability, since the surface stiffness will be positive definite in every direction. Similarly, if one uses the more realistic curtate-cycloid representation of the surface stiffness given by Eq. (11), the following inequality should be respected in order to achieve an absolute stability concerning the capillary term: $\Psi^{crt}=(1+\alpha)^2[m^2-(1+\alpha)^2]^{-1}$, which is also drawn in Fig. 3 as dashed lines, where the topography of the Wulff construction in 2D space is completely determined by two parameters: namely, the Wulff surface roughness parameter Ψ and the surface topography index number α. The last parameter fixes the shape of the stiffness function (the basic function for the Dirac δ singularity) at the cusp regions.

In Fig. 7, the electron wind intensity instability threshold level is plotted by utilizing Eq. (11) in connection with Eq. (31), assuming that there is no growth contribution $M_{vb}=0$, as a function of wave vector $k\subset[0\text{-}8\pi]$ and tilt angle $\phi\subset[0\text{-}\pi/2]$ for a fourfold rotational symmetry zone axis ⟨110⟩. From these figures one clearly observes the formation of an anomalous instability domain in the forbidden tilt angle interval denoted by $\phi\subset[0,\pi/4]$, which is normally controlled by the dissipative capillarity forces, when the WSR parameter exceeds the instability threshold level as illustrated graphically in Fig. 2. In fact, according to the 3D plots presented above, for high values of the Wulff surface roughness parameter such as $\Psi\cong 0.3$, the anomalous instability regime is not only stretched over the forbidden tilt angle sector, but also the normal instability domain shows extremely large enhancement by covering almost the whole region denoted by $\Psi\subset[\pi/4-\pi/2]$.

The first appearance of this new instability is solely due to the existence of negative spikes associated with the dimples of the surface stiffness profile. But the later stage of the anomalous instability, which shows stretching in the forbidden zone, is closely associated with the entrance of the surface stiffness to the negative values if the cusp regions are properly represented by the curtate-cycloid function in the Wulff polar construction, as mentioned and illustrated previously. Under normal circumstances, this tilt angle interval (the forbidden sector) for the fourfold symmetry zone axis should be under the influence of the usually observed capillary regime and should result in dissipative behavior in the growth phenomenon. The peculiarity of this anomalous instability domain comes from the fact that it does have an upper bond at very high wave numbers that may approach to infinity with the WST index number ($\alpha\rightarrow 1$), which is completely opposite to the usual electromigration-induced instability, where the instability is constrained only for small-wave-number (long-wave-surface-ripples) region, which has a well-defined upper bond. The same situation may be also said for the EM-induced stability domain above the capillarity threshold level, which does show an upper boundary that is extended deep into the high-wave-number region, as is hardly to be detected in Fig. 7. All these observations are the result of an analytical treatment of the surface stiffness. This anomalous instability regime shows itself even in the absence of an applied electric field, as may be seen from a close inspection of Fig. 7, which is not the case for the EM-induced instability boundary surface.

In the positive regions of the surface stiffness in the Wulff construction, the contribution of anisotropy to the total growth rate constant through capillarity would be a positive-definite cofactor regardless of the magnitude of the tilt angle, which means the capillarity still inhibits the enhancement of the surface disturbances. However, a close examination of Fig. 5 shows that even in a trigonometric representation of the surface Gibbs free energy the anisotropy in the surface stiffness still has an adverse effect on the stability compared to the isotropic case, because it causes not only an appreciable amount of short-wave entry into the instability domain, but also results a shift towards the upper boundary of the tilt angle $\phi\approx[\pi/m]$ in the basic interval.

According to Fig. 2, the upper bonds for the critical WSR parameters are given by $\Psi_2^{crt}\leqslant 0.65$, $\Psi_4^{crt}\leqslant 0.14$, and $\Psi_6^{crt}\leqslant 0.06$ for twofold, fourfold, and sixfold of symmetries, respectively. Hence, in general, the anisotropy in the surface Gibbs free energy has an adverse effect even in the absence of external forces such as EM or EDTI on the surface disturbances, for very well-defined ranges of the tilt angles, which is illustrated in Figs. 1 and 3. The situation gets worse at higher degrees of folding as clearly presented in Fig. 2.

The contribution of the EM effect to the surface disturbance growth rate depends upon the tilt angle, whether it inhibits instability or prefers enhancement of the surface disturbances. Therefore to interpret the combine effects of capillary and electromigration forces as functions of wave number and tilt angle by taking into account the complete anisotropy is very complicated in nature, even when one has

a very reliable analytical expression like that presented here. These difficulties may partially be surmounted with the aid of 3D graphical representations as introduced successfully in the present work.

In the presence of the above findings, the surface disturbance may be presented by the following transparent form rather than by Eq. (22):

$$h(x,t) = 1 + \bar{M}^0_{vb}(\sigma,T)(\Delta\bar{g}^0_{vb} + \bar{w}^0_b)t + \{a_\varepsilon \exp(\Gamma t)\exp[ik(x - \mathrm{v}_R t)] + \text{c.c.}\}, \quad (32)$$

where $\bar{M}^0_{vb}(\sigma,T)$ is the temperature- (Arrhenius) and stress-dependent normalized mobility. In the case of solid-phase epitaxial growth of ion-beam-amorphized Si and Ge, where the orientation of the crystal substrate can have a large influence on the growth rate in addition to the stress effect, it may be shown rigorously that the stress- and orientation-dependent transformation mobility denoted by $\bar{M}_{vb}(\sigma,\beta;T)$ takes part in the above equation. The propagation velocity given by expression (27) indicates that the surface disturbance moves along the applied electric field and its magnitude depends on the wave number linearly (dispersion) and the width of the interconnect. Its dependence on the tilt angle and the crystal symmetry described by the fold number $n = 2m$ is also very critical and strong.

B. Effect of the stress field on the instability of single-crystal thin films

According to the general formula denoted by Eq. (4), the elastic strain energy density contribution in the case of a solid-fluid interfacial layer may be given by $w_{b/\sigma} = \Omega_b \underline{\sigma}_{\sigma/b} \square \underline{\underline{S}}_b \square \underline{\sigma}_{\sigma/b}$ for a linear elastic solid, which is evaluated at the bulk phase just next to the surface layer. In writing Eq. (26), the following normalization procedure expression for the ESED has been considered by remembering the fact that the surface is assumed to be traction free during the solution of the elastic boundary value problem (this is definitely violated in the case of SPEG under hydrostatic pressure; otherwise, one cannot measure the $\lambda_{33} \equiv \hat{n} \cdot \underline{\underline{\lambda}} \cdot \hat{n}$ component of EDT):

$$\bar{w}_{b/\sigma} = (1 - \upsilon^2)\left(\frac{\sigma_h}{\sigma_0}\right)^2 \left(\frac{\sigma_0^2 \ell_0}{2E g^0_\sigma}\right) \equiv \Sigma_h \bar{\sigma}_h{}^2, \quad (33)$$

where $\Sigma_h \equiv (1-\upsilon^2)\left(\frac{\sigma_0^2 \ell_0}{2E g^0_\sigma}\right)$ is the strain energy intensity parameter (SEIP). This parameter represents the loading level under a uniaxial stress system, which is also used as a criterion for crack initiation or instability considerations. $\bar{\sigma}_h = \sigma_h/\sigma_0$ is the normalized hoop stress at the bulk phase adjacent to the surface layer. In Eq. (26), the gradient extraction operator ∂^C_x becomes very important in the first-order perturbation theory if there exist constant stress field gradients in addition to the oscillatory part of the field. This constant stress field gradient immediately contributes to the disturbance propagation velocity (phase velocity), similar to the electromigration far-field contribution represented by the second term in Eq. (26). For the present case, where the specimen is assumed to be loaded by an external uniaxial or biaxial stress system, the application of the extraction gradient operator returns zero and then no contribution to the disturbance phase velocity can be observed in LISA theory.

The effect of the elastic strain energy density on the instability may be calculated for a small perturbation rather easily. The results of the elastic boundary value problem solved by Asaro and Tiller[22] and Srolovitz[30] have unfortunately serious problems in their solutions for σ_{yy} and σ_{xy}. But later, using a more elegant and correct way by Gao[58,59] using the method originally developed by the celebrated Russian academician Muskhelishvili,[67] the hoop stress and the strain energy density at the interface may be rewritten in the following form using our adapted complex number representation:

$$\sigma_h \equiv \mathrm{Tr}\, \underline{\sigma}_{y=0} \cong \sigma_0(1 - 2\varepsilon k a_\varepsilon\{\exp[ik(x - \mathrm{v}t)] + \text{c.c.}\}) \quad (34)$$

and

$$\sigma_h^2 \cong \sigma_0^2(1 - \varepsilon 4 k a_\varepsilon\{\exp[ik(x - \mathrm{v}t)]\} + \text{c.c.}). \quad (35)$$

Similarly, the trace of the stress tensor, which is identically equal to the hoop stress in the traction-free surface, is given directly by Gao[59] in calculations, in addition to the deviatoric part of the stress tensor, where the global reference system is attached to the temporary position of the flat interface and the y axis is normal to the interface and directed towards the void phase (opposite to our adapted convention); then, one may write

$$\mathrm{Tr}\, \underline{\sigma} \cong \sigma_0(1 - 2k a_\varepsilon e^{ky}\{\exp[ik(x - \mathrm{v}t)] + \text{c.c.}\}). \quad (36)$$

Hence, the gradient of the trace of the stress tensor along the surface normal, which is pointed towards the bulk region, takes the following expression at the interface, $\bar{y}=0$, in scaled space;

$$\hat{n} \cdot \bar{\nabla}_2(\mathrm{Tr}\, \underline{\sigma}_{b/\sigma})|_{\bar{y}=0} = -\,\bar{y}\,(\mathrm{Tr}\, \underline{\sigma}_{b/\sigma})|_{\bar{y}=0} = +\,2\ell_0 a_\varepsilon \sigma_0 k^2\{\exp[ik(x - \mathrm{v}t)] + \text{c.c.}\}. \quad (37)$$

The above expression clearly indicates that under uniaxial tension, stress-assisted bulk diffusion prefers evaporation of the flat surface, where σ_0 and $w_0 = \sigma_0^2/2E$ are the uniaxial stress applied along the x axis and the elastic strain energy density at the flat interface, respectively. Note that according to our adapted profile, the strain energy density at the crest is lower than the trough. The surface or interfacial layer disturbance growth rate may be obtained from Eq. (26). Namely, the contributions due to the in-plane applied uniaxial stress system to the imaginary part of the propagation velocity may be calculated from the relationships (35)–(37) and assuming that the transformation mobility still does not depend on the applied stress field. Hence, one may write

$$\Gamma \equiv k v_{\mathrm{Im}} = -\{\chi m k^2 A \sin[2m\phi] + [1 + A\cos^2 m\phi]\hat{\gamma}(\pi/2,\phi)k^4 + (\Xi_s + 2\Sigma)[1 + A\cos^2 m\phi]2k^3\} - \{\bar{M}^0_{bv}[4\Sigma + \hat{\gamma}(\pi/2,\phi)k]k + \bar{M}_b \Xi_b 2k^2\}, \quad (38)$$

where $\Xi_s = (1+v)\frac{\ell_0\sigma_0}{3g^0_s}|\mathrm{Tr}\,\underline{\underline{\lambda}}^V_s|$ and $\Xi_b = (1+v)\frac{\ell_0\sigma_0}{3g^0_s}|\mathrm{Tr}\,\underline{\underline{\lambda}}^V_b|$ represent the elastic dipole interaction intensity parameters (EDIPs), respectively, in the interfacial layer and the bulk phase, assuming that the monovacancies or some other point-defect mechanisms (i.e., self-interstitial) are operating in both regions. The first group of terms accounts for the mass or particle transport in the surface layer, which is strictly valid for the interface between the solid and fluid phases. Here, the fluid phase also includes the amorphous solid state showing a high shear strain relaxation rate or creeping motion at high temperatures. The last group of terms between braces is associated with the phase transformation (the growth), and it is valid not only for surface layers but also for the interfacial layer between two condensed phases.

In this section, various contributions to the instability in the growth rate constant Γ and the phase velocity of surface disturbance are presented in great detail with factual interpretations supported by computer graphics based on published experimental data and derived from our analytical formulations elaborated in the previous sections. Especially, the various contributions of the applied stress system to the morphological evolution of free surfaces and interfaces are demonstrated for a prototype example such as a copper single-crystal solid thin-film interconnect line, and some references are made for the recrystallization of ion-beam-amorphized silicon, which will be also analyzed here in great detail since SPEG has been well documented experimentally in the literature.

The relationship (38) clearly shows that the contributions of the *elastic strain energy density*, represented by the Σ intensity parameter, to the disturbance growth rate constant Γ, due to the surface drift diffusion as well as for the phase transformation terms, are always negative definite (dissipation or healing effect) regardless of the wave number and the tilt angle. These findings due to the sign conflict in the generalized Gibbs free energy function[13] are just the opposite to some authors' conclusions that the strain energy density alone, above certain wave numbers, results in decay of the amplitude and otherwise causes surface roughness or instability. On the other hand, the situation with respect to EDIPs represented by Ξ_s and Ξ_b is completely different and distinct. The sign of these parameters depends on the sign of the applied stress system acting along the interfacial layer denoted by σ_0, whether it is uniaxial tension $\Xi > 0$ or compression $\Xi < 0$. Our LISA theory clearly shows that the EDT interaction, which appears in the surface drift diffusion, always favors surface smoothing when the solid phase is subjected to in-plane uniaxial tension, but in the case of uniaxial compression just the opposite phenomenon occurs: namely, the enhancement in the surface roughness takes place regardless of the wave number and the tilt angle. These findings are also in excellent agreement with the experimental results reported in the literature.[47,68] The situation with respect to the stress-assisted bulk diffusion is just the same, where the uniaxial compression favors the surface instability by the constantly supplying atomic flow to the crest regions and simultaneously draining atomic species from the trough regions with the same rate (conservative behavior having zero mean interface displacement) and causes the surface modulation to amplify rather than to decay. As far as the overall interface drift-diffusion contribution to the surface instability is concerned the sum over these two effects Σ and Ξ_s should be taken into account for the case of the uniaxial compression system. Actually, the combination of these two closely related or connected effects dictates the final contribution of the stress field on the instability (growth mode), which may be written as

$$\{(\Xi_s + 2\Sigma) + \hat{\gamma}(\pi/2,\phi)k\} = \frac{\sigma_0^2 \ell_0}{E g^0_\sigma}\left[1 - v^2 + (1+v)E\frac{\mathrm{Tr}\,\lambda^a_\sigma}{3\sigma_0}\right] + \hat{\gamma}(\pi/2,\phi)k < 0. \quad (39)$$

The above inequality may be easily handled, which results in the following instability (open) domain having well-defined upper and lower limits on the uniaxial stress system: namely,

$$0 > \sigma_0 > -(1-v)^{-1}E|\mathrm{Tr}\,\lambda^V_\sigma|/3 \quad (\text{instability bonds at } k = 0. \quad (40)$$

The above relationship for silicon[68] and copper[69] gives, respectively, the following figures: 21 GPa ($E=163$ GPa, $v=0.23$) and 15.65 GPa ($E=119$ GPa, $v=0.34$) for the lower threshold level in absolute magnitude value of the strain-energy-density-dominating regime, assuming that the trace of the EDT is in the range of $\mathrm{Tr}\,\underline{\underline{\lambda}} \cong 0.2-0.4$.

In Fig. 8 in the absence of electromigration forces, the stress-induced instability associated with the sidewall morphological evolution is presented for a hypothetical copper thin solid film ($h_0 = 10^{-6}$ M) having a texture $(111)\times[\bar{2}11]$ under uniaxial tension and compression, where instability hypersurfaces are plotted using the computer graphic facilities of MATCAD-13 in terms of the renormalized stress ($\hat{\sigma} \equiv \sigma/E_0$), the wave number k, and the tilt angle ϕ in parametric 3D space using Eq. (34). Here, three extreme values of the surface stiffness anisotropy constant, $B=0.02$, $B=1/17$, and $B=0.2$, are selected, respectively, well below and above the anomalous instability threshold level $B_{th}=1/17$ associated with the $\langle 111\rangle$ zone axis having sixfold rotational symmetry for the set of $\{10\bar{1}\}$ singular planes oriented along the $\phi = 30°, 90°, 150°$ directions. This system constitutes the most critical system as far as the morphological instability associated with the surface Gibbs free energy anisotropy is concerned.

As may be seen from Fig. 8(a) ($B=0.02$) and Fig. 8(b) ($B=1/17$), for low values of the anisotropy constant there is an absolute and well-defined instability subdomain embedded completely in the uniaxial compression region in the parametric space bounded by $[k=0, \phi=0]$ planes having an elevation characterized by the universal marginal stress level

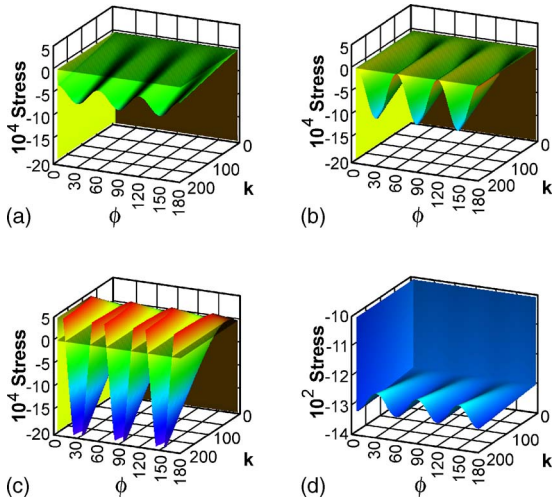

FIG. 8. (Color online) The stress-induced instability upper (a), (b), (c) and lower (d) bond hypersurfaces are plotted in terms of wave numbers $k:(0\text{-}2\pi)\Rightarrow\lambda:(0\text{-}h_0)$ and tilt angles (0-180°) for a EDT, $\mathrm{Tr}\,\underline{\lambda}=0.30$, using a set of selected surface stiffness anisotropy constants: namely, ($B=0.02$), ($B=1/17$), and ($B=0.20$), below and above the anomalous instability threshold level ($B_{th}=1/17$), for a top (111) surface having sixfold rotational symmetry, under applied uniaxial tension and compression along the $[\bar{2}11]$ direction, respectively, where the elastostatic data (Ref. 70) for a copper thin solid film having 1 μM thickness is used: $E_0=1.19\times10^{11}$ N M^{-2}, $\upsilon\cong0.34$, and $g_\sigma^0\cong1.6$ J M^{-2} (0.1 eV A^{-2}). The lower figures show the effects of the anomalous instability regime on the upper (c) and lower (d) boundary hypersurfaces. The maximum in the surface stiffness occurs at the tilt angles denoted by $\phi=30°$, 90°, and 150° and the negative spikes at $\phi=0°$, 60°, and 120° for this selected surface texture.

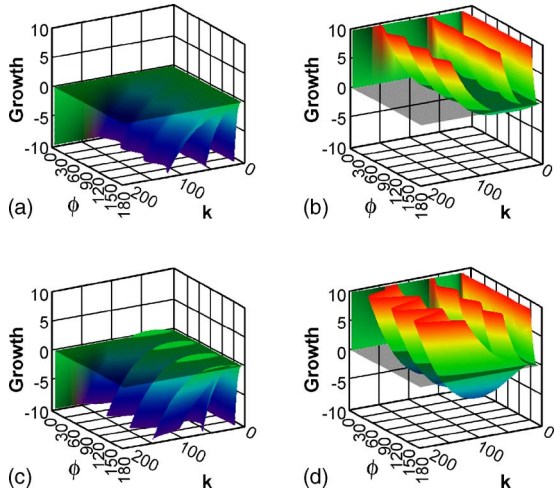

FIG. 9. (Color online) The instability growth rate constant Γ is plotted for three different renormalized stress levels given by $|\tilde{\sigma}|=10^{-5}$(1.19 MPa), $|\tilde{\sigma}|=10^{-4}$(11.90 MPa), and $|\tilde{\sigma}|=10^{-2}$(1.19 GPa) with respect to the wave number ($k=0\text{-}2\pi\Rightarrow\lambda=0\text{-}h_0$ and tilt angle for the sidewall surface morphological evolution of a copper single-crystal thin solid film having the (111) plane as a top surface with a thickness of 1 μM, under uniaxial tension and compression, respectively, using two selected surface stiffness anisotropy constants: namely below ($B=0.02$) and above ($B=0.1$), the anomalous threshold level given by $B=1/17$. The elastostatic data for copper (Ref. 70) is used: $E_0=1.19\times10^{11}$ N M^{-2}, $\upsilon=0.34$, $g_\sigma^0=1.6$ J M^{-2}, and $\mathrm{Tr}\,\lambda_\sigma^{\mathrm{Si}}\square0.3$.

presented in Fig. 8(d) denoted by $\tilde{\sigma}\equiv\frac{\sigma}{E}\leqslant-(1-\upsilon)^{-1}|\mathrm{Tr}\,\lambda_\sigma^V|/3$, which yields for copper and silicon $\tilde{\sigma}\cong-0.15$ and -0.13, respectively. The above calculated lower bound for the instability domain for copper indicates clearly that the stability may still prevail under the uniaxial compression because of the positive character of the strain energy density, and its negative contribution to the generalized bulk Gibbs free energy,[5,13] but its magnitude is so high that it can never be attained in practice for the vacancy-exchange mechanism of diffusion as postulated above having $|\mathrm{Tr}\,\lambda_\sigma^V|\cong0.3$. This gap in the renormalized stress level depends only on the elastic Poisson's ratio of the bulk phase and the trace of the EDT of the mobile atomic species. In the case of copper, the lower limit (in absolute magnitude) for the uniaxial compression above which stability may be observed in some well-defined regions is in the range of $|\sigma|\cong15.65$ GPa (156 kbar).

As far as the effects of the anomalous instability associated with the surface stiffness are concerned ($B\geqslant B_{th}$), they show themselves very clearly in Fig. 8(c) ($B=0.20$), where there are some absolute instability regions intruding into the uniaxial tension domain above the $\{k,\phi\}$ zero reference plane, which are stretching as wide strips all along directions of the $\phi=0°,60°,120°$ tilt angles, regardless of the magnitude of the wave number, where the surface stiffness takes negative values and the capillary forces no longer play the role of stabilizer. Similarly, the stability domain also penetrates into the compression region with increasing depth proportional to the wave number, along directions given by the tilt angles $\phi=30°,90°,150°$, which correspond to the maxima in the surface stiffness oriented along the direction of the cusps in the Wulff construction for the adapted texture mentioned previously. These are the important orientations, where the formation of strong faceting takes place. The present theory shows that they are extremely stable regardless of the sign of the applied stress system and the stability increases with wave number linearly even under uniaxial compression. Figure 8(d) ($B=0.20$) shows the lower-instability sheet beyond which the stability comes into play due to the positive influence of the elastic strain energy density, which contributes a negative term to the generalized Gibbs free energy density in the bulk region just adjacent to the interfacial layer,[5,6,13] as predicted previously. The strip widths of these anomalous stability and instability zones increase but never overlap with an increase in the instability constant denoted by $B\geqslant B_{th}$. The situation might be even worse if one considers the cusp formation represented by the curtate-cycloid curve along the vicinal planes as treated extensively in this paper.

In Fig. 9, the sidewall surface disturbance growth rate constants Γ are presented as 3D computer graphics as a function of wave number (0-2π) and tilt angle (0-180°) for three different applied stress systems, uniaxial tension, and compression, respectively, where the stress equilevel surface sheets in the compression side denoted by Figs. 11(b) and

11(d) rotate in the clockwise direction with an increase in the applied stress level and towards the anticlockwise direction in the case of uniaxial tension, Figs. 11(a) and 11(c). That means any increase in the applied stress level, whether it is tension or uniaxial compressive, always increases the absolute value of the growth rate constant of the surface modulations in the negative (roughness decay) or in the positive (roughness growth) directions, respectively. Under uniaxial compression the decay rate of the surface roughness increases with the applied stress level. According to Figs. 9(b) and 9(d), the system might show a stability region at the critical tilt angles $\phi=30°,90°,150°$ under very low applied compressive stresses for low values of the wave numbers and that region increases in extent drastically when the surface stiffness enters into the anomalous instability regime. Similar but just the opposite behavior may also be observed in Figs. 9(a) and 9(c) for low uniaxial tension loading, where the system shows instability at the critical tilt angles $\phi=0°,60°,120°$ and low wave numbers due to the negative surface stiffness spikes seen in Fig. 3, which are directly related to the maxima in the surface-specific Gibbs free energies.

It seems that there is an unanswered great puzzle associated with a novel experiment which was recently performed by Shreter *et al.*,[71] who observed unusual relief resembling *quasicracks on a compressionally stressed surface* of bent silicon subjected to chemical etching in the range of 814–200 MPa. But it is also strange that nothing took place on the opposite side, which was exposed to uniaxial tension at the same magnitude. This very revealing experiment is a strong indication that there is something seriously missing in the theory of Asaro, Tiller, and Grinfeld[22,72] (ATG) that cannot account for this strange behavior even when one has a reasonably high applied stress level. Of course this phenomenon has nothing to do with surface diffusion or evaporation condensation but the chemical removal of atoms. Similarly, in clean and free surfaces, according to the studies by Shenoy *et al.*,[73] the involvement of the adatom hopping motion might be possible and the rebounded [100]-oriented single-height step is strongly *stabilized by compressive strain* compared to most well-known step structures. The same group also claims that the (100) orientation is *unstable* under *compressive* stress from atomistic calculations on the self-assembly of Si-Ge quantum dots.[74] The last statement can be understood since there are several stretched bonds in this structure; one expects its energy to be lower in a compressive applied stress field than the tension.

Probably the most important mechanisms behind the interface stability are the stress- and orientation-dependent growth mobility, where the saddle point configuration of the mobile atomic species plays a profound role and the elastic dipole interaction of its distortion field with applied stress system takes a dominant position in the kinetics of the interfacial displacement reactions (i.e., for the recrystallization of amorphous silicon, SPEG), where one has experimental data on the interfacial layer of SPEG concerning EDT, which has tetragonal symmetry represented by $\lambda^*_{11}=\lambda^*_{22}\cong 0.14$, $\lambda^*_{33}\cong -0.56$, and $\mathrm{Tr}\,\lambda^*_{Si}=-0.28$. Therefore, the most critical situation is encountered in the application of LISA theory to the free surfaces, where one has not only complete uncertainty in

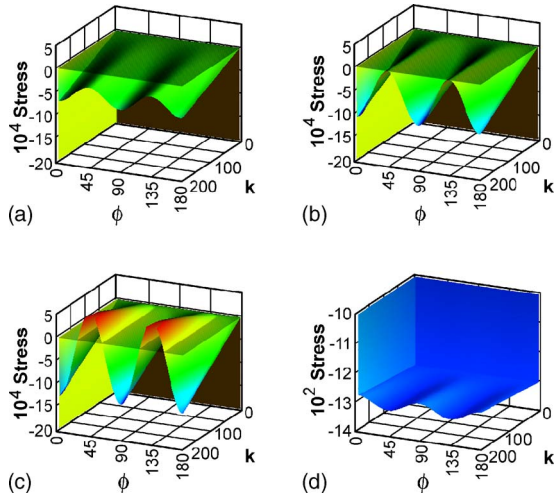

FIG. 10. (Color online) The stress-induced instability upper (a), (b), (c) and lower (d) bond hypersurfaces are plotted in terms of wave numbers $k:(0\text{-}2\pi)\Rightarrow\lambda:(0\text{-}h_0)$ and tilt angles (0-180°) for a EDT, $\mathrm{Tr}\,\underline{\lambda}=0.30$, using a set of selected surface stiffness anisotropy constants: namely, ($B=0.05$), ($B=1/7$), and ($B=0.50$), below and above the anomalous instability threshold level ($B_{th}=1/7$), for a fourfold rotational symmetry axis $\langle 1^{\pm}00\rangle$, under applied uniaxial tension and compression, respectively, where the elastostatic data (Ref. 75) for a silicon thin solid film having 1 μM thickness are used: $E_0=1.6\times 10^{11}$ N M^{-2}, $\upsilon=0.233$, and $g^0_\sigma=1.6$ JM^{-2}(0.1eVA^{-2}). The lower figures show the effects of the anomalous instability regime on the upper and lower boundary hypersurfaces.

the sign of the 2D trace $[\mathrm{Tr}\,\underline{\underline{\lambda}}\equiv(\lambda_1+\lambda_2)]$ of the EDT but also no sound quantitative experimental or theoretical information available in the literature on the individual in-plane eigenvalues associated with the mobile atomic species at the surface layer related to the adatom movements.

In Fig. 10, in the absence of electromigration forces, the stress-induced instability hypersurfaces of a silicon thin solid film ($h_0=10^{-6}$ M) under uniaxial tension and compression are plotted using the computer graphic facilities of MATCAD-13 in terms of the renormalized stress ($\hat{\sigma}\equiv\sigma/E_0$), the wave number k, and the tilt angle ϕ in parametric 3D space using Eq. (34), where three extreme values of the surface stiffness anisotropy constant, $B=0.05$, $B=1/7$, and $B=0.5$, are selected, respectively, well below, above, and at the anomalous instability threshold level $B_{th}=1/7$ for the fourfold symmetry zone axis $\langle 100\rangle$. As may be seen from Fig. 10(a) ($B=0.05$) and Fig. 10(b) ($B=1/7$) there is an absolute and well-defined instability subdomain embedded completely in the uniaxial compression region in the parametric space bounded by $[k=0,\phi=0]$ planes having an elevation characterized by the universal marginal stress level presented in Fig. 10(d) denoted by $\tilde{\sigma}\equiv\frac{\sigma}{E}\leqslant -(1-\upsilon)^{-1}|\mathrm{Tr}\,\lambda^V_\sigma|/3\cong -0.13$.

The above calculated lower bound for the instability domain for silicon indicates clearly that the stability may still prevail under the uniaxial compression because of the positive character of the strain energy density, and its negative contribution to the generalized bulk Gibbs free energy, but its magnitude is so high that it can never be attained in practice for the vacancy-exchange mechanism of diffusion as postu-

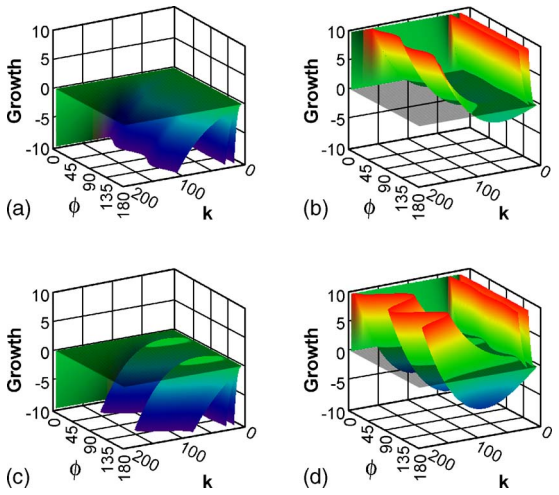

FIG. 11. (Color online) The instability growth rate constant Γ is plotted for three different renormalized stress levels $\{|\tilde{\sigma}|=10^{-5}(1.63\ \text{MPa}),\ |\tilde{\sigma}|=10^{-3}(163\ \text{MPa}),\ \text{and}\ |\tilde{\sigma}|=10^{-2}(1.63\ \text{GPa})\}$ with respect to the tilt angle $\phi=0$-$180°$ and wave number $k=0$-$2\pi \Rightarrow \lambda=0$-$h_0$ for a silicon single-crystal thin solid film having the (100) plane as a top surface with a thickness of 1 μM, under uniaxial tension and uniaxial compression, respectively, using two selected surface stiffness anisotropy constants below ($B=0.05$) and above ($B=0.25$) the anomalous threshold level given by $B=1/7$. The elastostatic data (Ref. 71) for silicon is used: $E_0=1.6\times10^{11}$ NM^{-2}, $\upsilon=0.233$, $g_\sigma^0=1.6$ JM^{-2}, and $\text{Tr}\,\lambda_\sigma^{\text{Si}}\square 0.3$.

lated above having $|\text{Tr}\,\lambda_\sigma^V|\cong 0.3$. This gap in the renormalized stress level according to the above-cited inequality is given by $[-0.130\leqslant\tilde{\sigma}_c\leqslant 0]$, and it depends only on the elastic Poisson's ratio of the bulk phase and the trace of the EDT of the mobile atomic species. In the case of silicon, the lower limit (in absolute magnitude) for the uniaxial compression above which stability may be observed in some well-defined regions is in the range of $|\sigma|=21$ GPa (210 kbar). In Fig. 11, the surface disturbance growth rate constants Γ are presented as 3D computer graphics as a function of wave number (0-2π) and tilt angle (0-180°) for three different applied stress systems, uniaxial tension, and compression, respectively, where the stress equilevel surface sheets in the compression side denoted by Figs. 11(b) and 11(d) rotate in the clockwise direction with an increase in the applied stress level and towards the anticlockwise direction in the case of uniaxial tension, Figs. 11(a) and 11(c). That means any increase in the applied stress level, whether it is tension or compressive, always increases the absolute value of the growth rate constant of the surface modulations in the negative (roughness decay) or in the positive (roughness growth) directions, respectively. Under uniaxial compression the decay rate of the surface roughness increases with the applied stress level. According to Figs. 11(b) and 11(d), the system might show a stability region under low applied compression for wave numbers and that region increases in extent drastically when surface stiffness enters into the anomalous instability regime. Similar but opposite behavior may also be observed in Figs. 11(a) and 11(c) for low uniaxial loading, where the system shows instability at the critical tilt angles ($\phi=45°,135°$) and for low wave numbers due to the negative surface stiffness spikes seen in Fig. 3.

IV. DISCUSSION

One should mention here that almost all of the arguments made about the surface morphological instability in the literature,[11,22,46,60] regardless of their sophistication in the calculation of the elastic strain energy density[38] or the temperature distribution due to the released of the latent heat of transformation,[76] strictly depend on the isotropic surface Gibbs free energy by presuming that the effects of the surface-specific Gibbs free energy anisotropy are negligible because the reported values of the anisotropy constant are very small.[77,78] On the other hand, the expression which dictates the boundary surfaces between stability and instability domains in the absence of electromigration, as presented by Eq. (39), shows clearly that the critical wavelength depends upon the orientation of the surface due to the surface stiffness elaborated in this paper. As far as the overall stress-gradient-induced interface drift-diffusion contribution to the surface instability is concerned the sum over these two effects—namely, $\Sigma\Rightarrow$ESED and $\Xi_s\Rightarrow$EDIP—should be taken seriously into account, especially in the case of the uniaxial compression system. Actually, the combination of these two closely correlated or, better to say, organically connected effects dictates the final contribution of the stress field on the *instability domain* (growth mode), which may be easily handled by introducing a new normalization scheme in terms of $\tilde{\sigma}=\sigma_0/E_0$ in connection with the definitions of these parameters given previously in Eqs. (3)–(33): then, after the conversion operation, one may write using Eq. (39) the following compact formula, which was also used in the production of the computer graphics in this paper:

$$(1-\upsilon^2)\tilde{\sigma}^2+(1+\upsilon)\tilde{\sigma}\frac{|\text{Tr}\,\lambda_\sigma^V|}{3}+\aleph\bar{\tilde{\gamma}}(\pi/2,\phi)k\leqslant 0\quad\text{(instability criteria)},\qquad(41)$$

where a new dimensionless parameter in real space, $\aleph=g_\sigma^0/E_0h_0$, is introduced, which may be called the *capillary stability enhancement factor* (CSEF) for good reason. This parameter, which clearly reveals the *hyperbolic size dependence* of the stability criteria for those objects under the applied or residual stress system, may be very important for nanoscale material systems. The high values of the CSEF encourages stability below the threshold level $B\leqslant B_{th}$ of the surface stiffness anomalous regime; otherwise, it may have adverse effects along those directions, where the surface stiffness becomes negative (the spikes in the Wullf construction). The equality sign gives the equation of the equilevel stress surfaces of two sheets, which partially encloses the instability domain in 3D parametric space, as extensively illustrated in Fig. 10. Outside of this domain, the surface disturbance decays. This expression clearly shows that there is a marginal uniaxial compressive stress region where the ESED dominates the overall behavior and results in surface undulations to decay rather than grow, which also appears in Fig. 10(d), and it is calculated as 20 GPA for a hypothetical silicon interconnect line. This region numerically is strongly correlated with the monovacancy relaxation or dilatation fields, $\text{Tr}\,\lambda_\sigma^V\equiv\delta\Omega_\sigma^V/\Omega_\sigma^a\leqslant 0$, at the surface layer as reported

by Emrick and McArdle[79] and Finnis and Sachdev,[80] where Ω_σ^a is the atomic volume in the unstrained matrix. Here, one should make it clear, in order to avoid any misconception, that the relaxed vacancy formation volume $\Omega_\sigma^V > 0$ is a positive quantity but the dilatation given by $(\Omega_\sigma^V - \Omega_\sigma^a)/\Omega_\sigma^a \leqslant 0$ is negative. This is an unfortunately highly confused point in the literature. The lower limit for the region, which is affected by the compressive stress adversely, can be also evaluated using the value given by Kirchheim[81] as $|\mathrm{Tr}\,\lambda_V^{Al}| = 0.2-0.4$ and $E^{Al} \cong 70$ GPa for aluminum, which results in $\sigma_{thres} = -7.6$ GPa (76 kbar), which is a very large compressive stress level to be reached in ordinary applications in order to inhibit the adverse effects due to EDTI by the contribution of ESED. Therefore, in practice EDTI-driven interfacial drift diffusion dominates the stability considerations on the surface disturbances. Similarly, one can estimate for aluminum the ESED and EDTI values for the 200-MPa nominal stress level observed in the passivated interconnect lines as $w_b^0 = 0.28$ J/cm^3 (2.9*E*-5 eV) and $u_{EDI} = 76$ J/cm^3 (7.8*E*-3 eV), respectively. These two figures show immediately that the elastic strain energy density compared to the elastic dipole tensor interaction energy is almost negligible. These energies are also too small compared to the mean thermal energy fluctuations $kT = 0.026$ eV even at room temperature. As a numerical example, the elastic dipole interaction energy for aluminum at the stress level given by $\sigma_0 = 1$ GPa is of the order of $u_{EDI} = 0.039$ eV, which is in the range of the thermal energy cited above. As stated on many occasions,[82] the elastostatic energies regardless of their nature it are too small compared to the physicochemical and electronic energies, which are mostly of the order of a few eV. The relationship denoted by $u/w = -2E\,\mathrm{Tr}\,\underline{\lambda}_\sigma \sigma_0^{-1}/3$ also shows that the elastic dipole interaction energy density dominates the strain energy density below a threshold stress level, which is about equal to 15 GPa for the present selected typical case.

As confirmed by the analysis of the experimental findings reported by Aziz *et al.*[41] and Lu *et al.*,[40] in silicon, the saddle point configuration for the activated complex atom at the interfacial layer definitely has tetrahedral symmetry. This may be due to the fact that the interfacial tension tensor as discussed recently by Ogurtani and Oren[5] is axisymmetric and the symmetry axis is oriented normal to the interface. The other important fact is that the interfacial tension tensor has positive and equal eigenvalues at the surface tangent plane and a negative eigenvalue (compressive) along the tetragonal axis. Of course, these eigenvalues may vary along the surface in the case of anisotropy. Lu *et al.*[40] have measured the pressure dependence of the solid-phase epitaxial growth rate Si into amorphous silicon produced by ion implantation SPEG and found that the activation volume has a negative sign and approximately $\mathrm{Tr}\,\lambda_a^* \Leftarrow \delta\Omega/\Omega = -28\%$ of the atomic volume. According to the activation complex theory developed in this paper for the generalized mobility associated with the phase transformation, the connection between the phenomenological activation volume and the EDT may be given by the following expression, where the third line in Eq. (13) is used in collaboration with Eqs. (14) and (17), which is, as stated above, valid for the recrystallization reaction well below the equilibrium temperature:

$$\Delta V_{ij}^*|_{def} = kT \left.\frac{\partial \langle \ln \mathrm{v}_d \rangle}{\partial \sigma_{ij}^{app}}\right|_T = kT \left\langle \left\{ \left.\frac{\partial \ln \hat{M}_{bv}}{\partial \sigma_{ij}^b}\right|_T + \frac{\partial \Delta \hat{g}_{bv}}{kT \partial \sigma_{ij}^b} \right\} \right\rangle$$
$$= \Omega_\sigma \langle \lambda_{ij}^* \rangle + \Delta_{bv} \langle \Omega_a \varepsilon_{ij} \rangle \cong \Omega_\sigma \langle \lambda_{ij}^* \rangle + \Omega_b S_{ijkl}^b \langle \sigma_{kl}^b \rangle. \quad (42)$$

While writing the last expression, we have assumed that there is complete stress relaxation in the reactant phase (amorphous Si) denoted by v. $\Delta V_{ij}^*|_{def}$ and $\langle \mathrm{v}_d \rangle$ are, respectively, the apparent activation volume determined experimentally and the absolute value of the mean interface displacement velocity, which is represented by the growth term in Eqs. (1) and (16). The term denoted by $\Delta_{bv}\langle \varepsilon_{ij} \rangle$ may be called the *transformation strain tensor* for the recrystallization process, the trace of which is closely related to the transformation dilatation $\Delta_{vb}\langle \mathrm{Tr}\,\varepsilon_{ij} \rangle = \langle \Delta \mathrm{v}/\mathrm{v} \rangle_{vb}$. Experimental determination of the activation volume relies on the applied remote in-plane stress system versus the interface displacement. Because of this, the value obtained from the above relationship represents not only the expectation or the mean value of the elastic dipole tensor of the activated complex state, but also some additional contribution due to transformation strain, which is actually a few orders of magnitude smaller than the EDT. Therefore, one may write $\mathrm{Tr}\,\Delta V_{ij}^*|_{def} \cong \Omega_\sigma \langle \mathrm{Tr}\,\lambda_{ij}^* \rangle = -0.28\Omega_\sigma$. The negative trace of the effective EDT associated with the mobile species at the saddle point configuration in the interfacial layer has far-reaching consequences in the case of applied hydrostatic compression. Later studies by Aziz *et al.*[68] are concentrated on nonhydrostatic stress effects on crystal growth kinetics in silicon system. They observed that the solid-phase growth rate of crystalline Si (001) from the amorphous Si on the tensile side is greater than on the compressive side of elastically bent wafers. According to the most recent studies by Barvosa-Carter and Aziz,[83] one of the in-plane activation volumes is $\Delta V_{11}^* = \Omega \underline{\lambda}_{11}^* = (0.14 \pm 0.04)\Omega$ due to the σ_{11} uniaxial stress system. This and previously reported findings in conjunction with the symmetry elements of the Si (001) plane are enough to determine the eigenvalues of the elastic dipole tensor, associated with the mobile activated complex atom at the saddle point configuration: namely, $\lambda_1 = \lambda_2 = 0.14$, $\lambda_3 = -0.56$, which amounts to $\mathrm{Tr}\,\underline{\lambda}^* = -0.28$ in the 3D elastic continuum. Using the transverse eigenvalue, the EDTI energy in crystalline Si may be calculated for an applied in-plane uniaxial compression stress given by $\sigma_{11} = -0.5$ GPa (5 kbar), which amounts to $u_{EDTI}^* = -\Omega_a \lambda_1 \sigma_{11} = 7.28 \times 10^{-3}$ eV. Similarly, the elastic strain energy per particle ESED for the same applied stress system is given by $w = \Omega_a \sigma_{11}^2/2E = 7.96 \times 10^{-5}$ eV. These two figures clearly show that the elastostatic energies regardless of their origin are very small compared to the activation energies, which are in the range of few electron volts for Si (2.68 eV) and Ge (2.17 eV). With the exception of very high applied hydrostatic stresses such as $|\mathrm{Tr}\,\sigma|/3 \geqslant 5$ GPa $\Rightarrow u_{EDT}^* \cong 0.028$ eV, the EDTI energy of the activated complex, compared to the mean thermal energy of $kT = 0.068$ eV, is about one order of magnitude smaller at the test temperature, which is about $T = 793$ K.

Therefore one has to take a different strategy for the factorization procedure of the generalized growth mobility. Namely, the stress-dependent reaction mobility should be factorized into *a nominal part* and *a perturbation part* after the decomposition of the local stress state into the stress for the flat interface $\underline{\underline{\sigma}}_0$ and the stress induced by the interface perturbations $\underline{\underline{\sigma}}_k$: namely, $\underline{\underline{\sigma}}=\underline{\underline{\sigma}}_0+\underline{\underline{\sigma}}_k$. Hence, one may perform the following very accurate linearization procedure after the proper factorization:

$$\bar{M}_{vb}(\beta,\underline{\underline{\sigma}};T)=\bar{M}^0_{vb}(\beta,\underline{\underline{\sigma}}_0;T)\exp\left\{\frac{\Omega\underline{\underline{\lambda}}^*_\sigma\otimes\underline{\underline{\sigma}}_k}{kT}\right\}$$
$$\cong\bar{M}^0_{vb}(\beta,\underline{\underline{\sigma}}_0;T)\left[1+\frac{\Omega\underline{\underline{\lambda}}^*_\sigma\otimes\underline{\underline{\sigma}}_k}{kT}\right]. \quad (43)$$

Utilizing the above approximation for the normalized mobility, in the formulation of the growth term in Eq. (25), one can obtained the following identity by employing the calculated surface stress distribution given by Eqs. (34)–(37) for the in-plane uniaxial stress system. Hence

$$\bar{M}_{vb}(\beta,\sigma;T)[\Delta\bar{g}_{bv}+\bar{\bar{\gamma}}(\pi/2,\phi)h_{xx}]\cong\bar{M}^0_{vb}(\beta,\underline{\underline{\sigma}}_0;T)$$
$$\times\left\{\frac{\Omega\sigma^0_{11}\lambda^*_{11}}{kT}[(\Delta\bar{g}^0_{bv}+\bar{w}^0_b-2\Sigma k-\bar{\bar{\gamma}}(\pi/2,\phi)k^2)]\right.$$
$$\left.-[2\Sigma k+\bar{\bar{\gamma}}(\pi/2,\phi)k^2]+[\Delta\bar{g}^0_{bv}+\bar{w}^0_b]\right\}. \quad (44)$$

During the derivation of the above connection, one still stays in the domain of the validity of the first-order perturbation theory. The part of the first term combined with the third term in the above expression should replaced by the similar term in Eq. (32) in order to obtain the following more accurate expression for the surface profile displacement dynamics including the phase transition:

$$h(x,t)=h_0+\bar{M}_{vb}(\beta,\underline{\underline{\sigma}}_0;T)(\Delta\bar{g}^0_{bv}+\bar{w}^0_b)t$$
$$+\{a_\varepsilon\exp(\Gamma t)\exp[ik(x-\mathrm{v}_R t)]+\mathrm{c.c.}\} \quad (45)$$

and

$$\bar{M}_{vb}(\beta,\sigma_0;T)\cong\bar{M}^0_{vb}(\beta,\underline{\underline{\sigma}}_0;T)\exp\left[\frac{\Omega\sigma^0_{11}\lambda^*_{11}}{kT}\right]. \quad (46)$$

The beautiful part of relationship (45) is that the interface *mean displacement velocity* given by $\bar{M}_{vb}(\beta,\underline{\underline{\sigma}}_0;T)(\Delta\bar{g}^0_{bv}+\bar{w}^0_b)$ depends only on the applied remote static nominal stress system; therefore, it is time independent as long as $\Delta\bar{g}^0_{bv}$ stays uniform in space (homogeneous temperature distribution at the interface) and constant in time (quasistatic or steady-state phase transformation), which is the case for the isothermal phase transitions of single-component systems, where in the case of the applied hydrostatic stress system one should consider the following replacement: $\sigma^0_{11}\lambda^*_{11}\Rightarrow\mathrm{Tr}\,\underline{\underline{\sigma}}\,\mathrm{Tr}\,\underline{\underline{\lambda}}/3$ (see the Appendix). Similarly the combination of the first and second terms in Eq. (44) replaces the growth term due the phase transition in Eq. (38). All these legal mathematical manipulations finally result in the following relationship for the instability growth rate Γ of the pre-existing surface disturbances and morphology evolutions under electromigration and elastostatic forces (uniaxial in plane) by taking full account of the orientation and stress dependence of the generalized growth mobility denoted as $\bar{M}_{vb}(\beta,\underline{\underline{\sigma}}_0;T)$:

$$\Gamma\equiv k\mathrm{v}_{\mathrm{Im}}\cong-\chi mk^2A\sin[2m\phi]-[(\Xi_s+2\Sigma)+\bar{\bar{\gamma}}(\pi/2,\phi)k]$$
$$\times[1+A\cos^2 m\phi]k^3-\{\bar{M}_b\Xi_b 4k^2+\bar{M}^0_{bv}(\beta,\sigma_0)(1+\Xi_M)$$
$$\times[2\Sigma+\bar{\bar{\gamma}}(\pi/2,\phi)k]k\}, \quad (47)$$

where we have introduced another new parameter $\Xi_M\equiv\Omega\sigma^0_{11}\lambda^*_{11}/kT\ll1$, which may be called the *stress-induced growth mobility enhancement* (SIGME) factor. SIGME combined with unity may be put into exponential format, which gives back to the generalized growth mobility denoted as $\bar{M}_{vb}(\beta,\sigma_0;T)$ similar to Eq. (46). In the case of SPEG, this parameter is positive for the in-plane uniaxial tension and negative for the compression, since the in-plane eigenvalues of the EDIT are positive ($\lambda^*_{11}=\lambda^*_{22}\cong0.14$). The above formula (47), in connection with the interface displacement (growth) relationship given by Eq. (45), clearly indicates that the SIGME parameter affects not only the kinetics of the phase boundary mean displacement velocity during the phase transformation—by retarding under the uniaxial compression or enhancing in the case of uniaxial tension—but also has influence on the stability of the morphological evolution of surfaces. According to the last group of terms in Eq. (47), the SIGME factor, depending upon the sign of the surface tension, may inhibit or enhance the stability, which is described by the growth rate constant expression, explicitly. Namely, below the threshold level of the anomalous surface stiffness regime it enhances the stability in the case of uniaxial tension and retards it otherwise, since its cofactor is positive regardless of the tilt angle and wave number. On the other hand, in the anomalous surface stiffness instability regime, as we discussed previously, everything depends upon the tilt angle and wave number, rather strongly. Definitely the stability is drastically encouraged for the vicinal planes $\langle100\rangle$, where there is a strong tendency for the occurrence of faceting observed in naturally grown crystals and inhibited for the $\langle11^{\pm}0\rangle$ direction due to the appearance of negative spikes in the Wulff construction of the surface Gibbs free energy. The direction of the morphological instability of an interface is also connected with the direction of the stress-assisted interfacial diffusion, which is given by $\nabla_2(\Omega\lambda_{11}\sigma_{11})$, which means that uniaxial tension according to the term Ξ_s in Eq. (47) decreases the amplitude (stability) of the surface modulation and the compression increases it (instability) as long as $\lambda_{11}\geqslant0$.

In order to give an additional experimental justification of LISA theory, one can easily calculate the stress enhancement factor for the applied pressure $p=3.2$ GPa at the test temperature 550 °C, which is employed by Lu *et al.*,[40] for the Si-SPEG specimen, where a factor of 5 enhancement in the growth rate is observed over 1 atm pressure. Namely, one obtains the following result: $\exp(-\Omega_a\,\mathrm{Tr}\,\underline{\underline{\lambda}}^*p/kT)\cong4$, where

$\mathrm{Tr}\,\underline{\underline{\lambda}}=0.28=-\delta\Omega_a/\Omega_a$ (contraction), which is in excellent agreement with the reported value of 5.

The anisotropy in the growth rate associated with the orientation of the interface is embedded in the mobility that contains the nominal stress effect in our previous discussion, which may be easily factorized out using the extensive experimental studies by Csepregi *et al.*:[45] namely,

$$\bar{M}^{0}_{bv}(\beta,\underline{\underline{\sigma}}_0)\equiv[1+(a_{100}-1)|\sin(\alpha-\beta)|/\sin(\beta)]\bar{M}^{111}_{bv}(\underline{\underline{\sigma}}_0), \tag{48}$$

where $\alpha=54.74^{\circ}$ is the angle between the (100) and (111) planes and β is defined as the angle between the $\langle 100\rangle$ direction and the surface normal of the substrate over which SPEG has been tested. According to data supplied by the above-mentioned reference, one has $a_{100}=19.7$ and $a_{100}=15$ for Si and Ge, respectively, at the temperature of one-half the melting point, where $\bar{M}^{111}_{bv}(\underline{\underline{\sigma}}_0)$ is the nominal stress-dependent mobility for the (111) plane.

Unfortunately, in this paper we have not treated thoroughly the effects of the mesoscopic-scale temperature nonuniformity on the interface instability, which may be invoked by the Joule effect due to current crowding and /or the localized heat released in the case of exothermic reactions occurring at the interfacial layers during the phase transformation taking place in the undercooled state (regrowth of SPEG). This is due to the lack of a simple, manageable, and reliable analytic expression to be used for the simulation of realistic laboratory test conditions, which are mostly done under gross isothermal conditions. However, for the quasistatic temperature distribution at the liquid-solid (i.e., crystalline-amorphous silicon) interface, as a naive approach one may utilize, similar to the Mullins-Sekerka[76,84] theory, the so-called *capillary formula* in connection with Eq. (47), which is given by $T_\sigma/T_m=(1+\kappa\mathfrak{J})$ using our adapted sign convention for the local curvature $\bar{\kappa}$ where $\mathfrak{J}\equiv(g_\sigma/L_\sigma)$ and $L_\sigma\equiv\Delta h_{bv}\geqslant 0$ is the volumetric latent heat of solidification (i.e., recrystallization). This formula can be easily deduced from the master equation (1) by taking the generalized force for the growth term denoted by the expression $[\Delta\bar{g}_{bv}+\bar{\bar{\gamma}}(\hat{\theta},\phi;m)\bar{\kappa}]\equiv\Delta\bar{h}_{bv}-T\Delta\bar{s}_{bv}+\bar{\bar{\gamma}}(\hat{\theta},\phi;m)\bar{\kappa}\Rightarrow 0$ as equal to zero (reversibility) and then assuming that the entropy $\Delta\bar{s}_{bv}$ and the enthalpy $\Delta\bar{h}_{bv}$ of transformation are independent of temperature and local curvature. That also results in a simple and familiar connection $\Delta\bar{s}_{bv}\cong\Delta\bar{h}_{bv}/T_m$. Of course this approach is strictly valid for reversible or equilibrium phase transformations and reactions. After some rearrangements of the terms and using the definition of $\bar{\Upsilon}$ appearing in Eqs. (1) and (2), the following mathematically more sound expression may be easily deduced for the surface particle flux contribution to the instability criteria due to the combined effects of the capillarity and the thermomigration (Soret effect) invoked by the nonuniform temperature profile created by the heat released at the interface during the reversible phase transformation in normalized space—that is,

$$\partial_x[-\Upsilon_\sigma\bar{T}_\sigma+\bar{\bar{\gamma}}(\cdot)f^3(h_x)h_{xx}]\Rightarrow[1-\mathrm{ThM}^\sigma]\bar{\bar{\gamma}}(\cdot)\partial_x f^3(h_x)h_{xx}, \tag{49}$$

where $\mathrm{ThM}^\sigma=(s^\sigma_T T_m/\Omega_\sigma L_\sigma)$ is a dimensionless parameter, which may be called the *latent-heat-induced thermomigration* (LHITM) intensity parameter. In the final stage of the treatment, the above relationship enters exactly as a cofactor $[1-\mathrm{ThM}^\sigma]$ for the orientation-dependent part of the surface stiffness in the second line of Eq. (47). One may also see immediately that the temperature is lower at the crest $\{\kappa\leqslant 0\}$ than the trough $\{\kappa\geqslant 0\}$ for exothermic transformations. This means the direction of the atomic flow due to thermal drift diffusion should be from the trough regions towards the crests, which eventually amplifies the interface roughness. The simple relationship (49) obtained in this paper tentatively tells us that the thermomigration invoked by the exothermic phase transformations occurring during the interface displacement reduces the intensity of the capillary forces. That means LHITM, below the anomalous surface stiffness threshold level, enhances the instability by reducing the positive role of the capillarity and in the anomalous regime just the opposite occurs, and it tries to encourage stability by exactly the same reason. The endothermic reaction acts in just the opposite direction and enhances the capillary forces. Actually, in practice, for a meaningful stability analysis, one has to solve numerically two coupled moving-boundary-value problems (MBVP's), respectively, associated with the time-dependent heat generation and dissipation governed by *ad hoc* thermokinetics laws and the boundary displacement or the surface evolution events, which are controlled by the law of irreversible thermodynamics as described, as a well-posed MBVP in Eq. (1) supplemented by auxiliary well-defined boundary conditions, even for the triple-junction singularities.[5,6,48] A very recent work reported by Huang *et al.*[85] on the composite SnPb flip-chip solder joints showed that migration of the Sn-rich phase in the contact area is caused by thermomigration in the lateral direction owing to the existence of a localized hot spot at the current crowding region. Finally, the partial melting at the Sn-rich region occurs due to a large Joule heating at the end of the void growth before an electrical opening takes place. This shows the nanoscale technological importance of adding new terms associated with the thermomigration-driven surface and bulk drift diffusion into master equations (1) and (18) rather rigorously in order to establish a sound framework for future computer experiments to reveal these detrimental effects thoroughly, similar to electromigration-invoked reliability considerations.[4,16,17]

V. CONCLUSIONS

The present unified theory of the irreversible thermodynamics of interfaces and surfaces, having multicomponent chemical species, gives a more elegant and generalized approach to LISA by transforming the governing equation into a more manageable quasilinear partial differential equation format including evaporation and condensation terms, while keeping in mind that our primary objective is to collect and

manipulate only the first-order perturbation contributions at the final stage. This unique *a priori* approach results an extreme simplification of the calculation machinery and also gives great flexibility to deal with anisotropy in the diffusivity as well as in the specific Gibbs surface energy (i.e., surface stiffness). Especially, the Dirac δ distribution singularity in the surface stiffness at the cusp regions of the Gibbs free energy profile (singular or vicinal planes) in the Wulff construction is treated in a unique way by utilizing the modified curtate-cycloid function as a basis function. This rigorous mathematical treatment in the present context allows us to deal with this intricate problem analytically as well as numerically with any degree of accuracy, above and below the roughening temperature with a slight modification. The anomalous instabilities associated with the capillary term in certain ranges of the tilt angle are also elaborated and demonstrated by computer graphics, which might help better understand the importance of cusps on the faceting and growth kinetics of surface disturbances quantitatively.

This unified theory successfully brought together the various effects on the morphological evolutions of surfaces and interfaces due to the applied stress systems and electrostatic forces, even thermomigration formally in a systematic fashion, by combining the irreversible thermodynamics of surfaces and interfaces with the quasithermokinetics theory of activation complexes in the formulation of the generalized stress- and orientation-dependent growth mobility. In this way, the anisotropy combined with stress influence, not only in the thermodynamic functions, but also in the kinetic parameters such as the generalized mobilities, revealed themselves to such an extent that one can make quantitative predictions of the behavior of the composite system during the evolution process. The effects of the anomalous instability regime associated with the surface stiffness on the stressed-induced morphological evolution are explored by 3D graphics, which showed extremely interesting scenarios by minor variations in the surface-specific Gibbs free energy (SSGFE) anisotropy constant. The present work without hesitation shows that it is a great misconception to underestimate the profound role of the SSGFE anisotropy because of its extremely low variation range[53,54] ($B \cong 0.1-0.5$) compared to the similar anisotropy associated with the surface drift-diffusion coefficients, which may vary a few orders of magnitude with the tilt angle ($A \cong 1-10^3$).

Even though the present theory relies on a first-order perturbation approach, still our very recent extensive simulation studies (192 different configurations in the parametric space), respectively, on the finite-Gaussian-shape edge-hillock and edge-void perturbations on the otherwise flat sidewall surfaces of thin solid single-crystal films have proven that LISA has great predictive power even in the nonlinear region of instability under electromigration forces having strong diffusional anisotropy, with few exceptions: namely, bifurcation points, where the system goes from the stability domain to instability regime or vice versa.[86,87]

Finally, one may state without hesitation that the elastic dipole tensor interaction EDTI that was originally advocated by Kröner,[88] and extensively employed by Ogurtani and Seeger[89] in a series of papers dealing with the theory of the internal friction spectrum associated with the interaction between dislocation kink chains and the atmosphere of mobile paraelastic atomic defects in bcc metals has more profound qualitative as well as quantitative effects on the morphological evolutions of the surfaces and interfaces between two condensed phases than the elastic strain energy density ESED, as has been demonstrated in this paper.

ACKNOWLEDGMENTS

The author thanks William D. Nix of Stanford University and Dick Bedeaux of Norwegian University of Science and Technology, Trondheim for their constant interest in our recent theoretical work on the surfaces and interfaces. Thanks are also due Lucien Brush and Emre Ersin Oren of the University of Washington, Seattle, allowing me to see their remarkable work on the LISA theory before its publication, which inspired me to elaborate on the topic further. This work was partially supported by the Turkish Scientific and Technical Research Council, TUBITAK, through a research Grant No. 104M399.

APPENDIX

The tetrahedral (axisymmetric) elastic dipole tensor may be described by the format $\{\underline{\underline{\lambda}}^{*}_{\hat{q}}=\lambda_1[\underline{\underline{I}}+\eta\delta_{(n)q}\delta_{(n)m}]\}$, where $q=3$ denotes direction of the symmetry axis and $\eta=(\lambda_3-\lambda_1)/\lambda_1$, which is closely related to the shape factor.[89] $\lambda_3,\lambda_1=\lambda_2$ are the principal values of the tetragonal elastic dipole tensor, along the symmetry axis denoted by $\hat{q}$ and in the interface tangent plane (transverse components), respectively. $\delta_{(n)q}$ is the Kronecker delta function, $\hat{q}\square\hat{n}$ denotes the direction of the tetragonal axis, which is parallel to the interface normal $\hat{n}$ for the present case, and $(\cdot)$ indicates that the Einstein summation rule for the repeated indices is not valid. Then one can easily show that the EDTI energy may be given by the expression $u^{*}_{EDI}=-\Omega\lambda_1(\mathrm{Tr}\,\underline{\underline{\sigma}}+\eta\sigma_{qq})$ for the general applied stress system, where $\sigma_{qq}\equiv\hat{q}\cdot\underline{\underline{\sigma}}\cdot\hat{q}$, and it is equal to zero for the traction-free surfaces. However, it is finite for the composite system under a hydrostatic stress field such as the isotropic pressure $\sigma_{qq}\equiv -p$. The nonvanishing shape factor η of EDT may have a very important contribution to the EDTI energy, especially in the case of the pure deviatoric stress system $\mathrm{Tr}\,\underline{\underline{\sigma}}=0$, where the stress tensor component along the tetragonal axis denoted by σ_{33} appears as an only contribution to the interaction energy. The above formula clearly shows that one cannot consider the application of the pure hydrostatic stress (whether it is hydrostatic pressure or triaxial tension) $\underline{\underline{\sigma}}=-p\underline{\underline{I}}$ on the composite system (solid/fluid and solid/amorphous), without violating the mostly used traction-free boundary condition, where the realistic boundary condition may be specified as a shear-free interface, which is given by $\sigma_{qt}\equiv\hat{n}\cdot\underline{\underline{\sigma}}\cdot\hat{t}=0$. The principal eigenvalue of EDT, λ_3, can only be measurable if the traction-free elastic constraint at the dividing interface is lifted. Then the following expression results for the EDT interaction: $u^{*}_{EDI}=\Omega p(\lambda_3+2\lambda_1)$. Therefore, not only the

hydrostatic but also the deviatoric part of the stress system can interact with the axisymmetric (tetragonal) elastic dipole tensor if it has a nonvanishing component σ_{nn} along the surface normal. In the case of the biaxial stress system acting in the surface tangent plane one can obtain the following expression for the EDTI energy: $u^{*}_{EDI}=-2\Omega\lambda_1\sigma_{11}$. This shows that the biaxial in-plane stress has twice the effect of uniaxial stress as confirmed experimentally by Hong *et al.*[90]

*Corresponding author. FAX: +90-312-210-1267. Electronic address: Ogurtani@metu.edu.tr (Url: http://www.csl.mete.metu.edu.tr).

[1] D. Bedeaux, Adv. Chem. Phys. **64**, 47 (1986).
[2] Y. D. Shikhmurzaev, J. Fluid Mech. **334**, 211 (1997).
[3] D. Bedeaux, J. Chem. Phys. **120**, 3744 (2004).
[4] T. O. Ogurtani and E. E. Oren, J. Appl. Phys. **96**, 7246 (2004).
[5] T. O. Ogurtani and E. E. Oren, Int. J. Solids Struct. **42**, 3918 (2005).
[6] T. O. Ogurtani, J. Chem. Phys. **124**, 144706 (2006).
[7] Z. Suo, Adv. Appl. Mech. **33**, 193 (1997).
[8] D. A. Saville, J. Chun, J. L. Li, H. C. Schniepp, R. Car, and I. A. Aksay, Phys. Rev. Lett. **96**, 018301 (2006).
[9] J. Krug and H. T. Dobbs, Phys. Rev. Lett. **73**, 1947 (1994).
[10] M. Schimschak and J. Krug, Phys. Rev. Lett. **78**, 278 (1997).
[11] M. Schimschak and J. Krug, J. Appl. Phys. **87**, 695 (2000).
[12] M. R. Gungor and M. Maroudas, J. Appl. Phys. **85**, 2233 (1999).
[13] T. O. Ogurtani and E. E. Oren, J. Appl. Phys. **90**, 1564 (2001).
[14] E. E. Oren and T. O. Ogurtani, in *Thin Films: Stresses and Mechanical Properties IX*, edited by C. S. Ozkan, R. C. Cammaratai, L. B. Freund, and H. Gao, MRS Symposia Proceedings No. 695 (Materials Research Society, Pittsburgh, 2002), p. L.5.51.
[15] M. Nathan, A. Averbuch, and M. Israeli, Thin Solid Films **466**, 347 (2004).
[16] T. O. Ogurtani and O. Akyildiz, J. Appl. Phys. **97**, 093520 (2005).
[17] T. O. Ogurtani and O. Akyildiz, in *Materials, Technology and Reliability of Low-k Dielectrics and Copper Interconnects*, edited by T. Y. Tsui, Y-C. Joo, A. A. Volinsky, M. Lane, and L. Michaelson, MRS Symposia Proceedings No. 914 (Materials Research Society, Warrendale, PA, 2006), p. 0914-F09-22.
[18] R. M. Bradley, Phys. Rev. E **60**, 3736 (1999).
[19] P. G. Drazin and R. S. Johnson, *Solitons: An Introduction* (Cambridge University Press, Cambridge, England, 1989), p. 9.
[20] M. Mahadevan, R. V. Bradley, and J.-M. Debierre, Europhys. Lett. **45**, 680 (1999).
[21] T. O. Ogurtani (unpublished).
[22] R. J. Asaro and W. A. Tiller, Metall. Trans. A **3**, 1789 (1972).
[23] C. Herring, in *The Physics of Powder Metallurgy*, edited by W. E. Kinston (McGraw-Hill, New York, 1951), p. 143.
[24] E. A. Guggenheim, *Thermodynamics*, 3rd ed. (North-Holland, Amsterdam, 1959), p. 46.
[25] H. B. Callen, *Thermodynamics* (Wiley, New York, 1960), p. 237.
[26] H. H. Yu and Z. Suo, J. Appl. Phys. **87**, 1211 (2000).
[27] J. Rice and T. J. Chuang, J. Am. Ceram. Soc. **64**, 46 (1981).
[28] Z. Suo and W. Wang, J. Appl. Phys. **76**, 3410 (1994).
[29] M. R. Gungor and D. Maroudas, Int. J. Fract. **109**, 47 (2001).
[30] D. J. Srolovitz, Acta Metall. **37**, 621 (1989).
[31] C. Herring, J. Appl. Phys. **21**, 437 (1950).
[32] H. Gao, Int. J. Solids Struct. **28**, 703 (1991).
[33] N. I. Muskhelishvili, *Some Basic Problems of the Mathematical Theory of Elasticity* (Noordhoff, Groningen, 1953), p. 104.
[34] Yu. G. Shreter, D. V. Tarkhin, S. A. Khorev, and Yu. T. Rebane, Phys. Solid State **41**, 1295 (1999).
[35] W. B. Hillig and R. J. Charles, in *High-Strength Materials*, edited by V. F. Zackay (Wiley, New York, 1965), p. 682.
[36] T. J Chuang and E. R. Fuller, J. Am. Ceram. Soc. **75**, 540 (1992).
[37] B. J. Spencer, P. W. Voorhees, and S. H. Davis., Phys. Rev. Lett. **67**, 3696 (1991).
[38] B. J. Spencer, S. H. Davis, and P. W. Voorhees, Phys. Rev. B **47**, 9760 (1993).
[39] M. A. Grinfeld, Dokl. Akad. Nauk SSSR **290**, 1358 (1986) [Sov. Phys. Dokl. **31**, 831 (1989)].
[40] G. Q. Lu, E. Nhgen, M. J. Aziz, D. Turnbull, and C. W. White, Appl. Phys. Lett. **54**, 2583 (1989).
[41] M. J. Aziz, P. C. Sabin, and G. Q. Lu, Phys. Rev. B **44**, 9812 (1991).
[42] R. J. Rice, J. Mech. Phys. Solids **19**, 433 (1971).
[43] W. Barvosa-Carter and M. J. Aziz, Phys. Rev. Lett. **81**, 1445 (1998).
[44] E. N. Yeremin, *The Foundations of Chemical Kinetics* (MIR, Moscow, 1979), p. 233.
[45] L. Csepregi, E. F. Kennedy, and J. W. Mayer, J. Appl. Phys. **49**, 3906 (1978).
[46] J. Liang and Z. Suo, Interface Sci. **9**, 93 (2001).
[47] W. Barvosa-Carter, M. J. Aziz, A. V. Phan, T. Kaplan, and L. J. Gray, J. Appl. Phys. **96**, 5462 (2004).
[48] T. O. Ogurtani, Phys. Rev. B **73**, 235408 (2006).
[49] R. Haase, *Thermodynamics of Irreversible Processes* (Addison-Wesley, Reading, MA, 1969), p. 377.
[50] H. Wever, *Electro und Thermotransport in Metallen* (Johann Ambrosius Barth, Leipzig, 1973).
[51] R. Kirchheim and U. Kaeber, J. Appl. Phys. **70**, 172 (1991).
[52] S. R. De Groot, *Thermodynamics of Irreversible Processes* (North-Holland, Amsterdam, 1961), p. 114.
[53] W. Wang and Z. Suo, J. Mech. Phys. Solids **45**, 709 (1997).
[54] L. E. Murr, *Interfacial Phenomena in Metals and Alloys* (Addison-Wesley, London, 1975), p. 186.
[55] *CRC Standard Mathematical Tables*, 3rd ed., edited by S. M. Shelby (The Chemical Rubber Co., Cleveland, OH, 1973), p. 389.
[56] V. S. Vladimirov, *Generalized Functions in Mathematical Physics* (MIR, Moscow, 1979), p. 8.
[57] Y. C. Fung, *Foundations of Solids Mechanics* (Prentice-Hall, Englewood Cliffs, NJ, 1965), p. 358.
[58] H. Gao, in *Modern Theory of Anisotropic Elasticity and Applications*, edited by J. J. Wu, T. C. T. Ting, and D. M. Barnett (SIAM, Philadelphia, 1991), p. 139.
[59] H. Gao, Int. J. Solids Struct. **28**, 703 (1991).
[60] M. J. Aziz, P. C. Sabin, and G. Q. Lu, Phys. Rev. B **44**, 9812 (1991).

[61] L. Onsager, Phys. Rev. **37**, 405 (1931).
[62] L. Onsager, Phys. Rev. **38**, 2265 (1931).
[63] T. O. Ogurtani and A. K. Seeger, J. Chem. Phys. **79**, 5041 (1983).
[64] E. N. Yeremin, *The Foundations of Chemical Kinetics* (MIR, Moscow, 1979), p. 233.
[65] M. Hillert, Acta Metall. **13**, 227 (1965).
[66] L. Brush and E. E. Oren (unpublished).
[67] N. I. Muskhelishvili, *Some Basic Problems of the Mathematical Theory of Elasticity* (Noordhoff, Groningen, 1953), p. 104.
[68] M. J. Aziz, P. C. Sabin, and G. Q. Lu, Phys. Rev. B **44**, 9812 (1991).
[69] A. Witvrouv and F. Spaepen, J. Appl. Phys. **74**, 7154 (1993).
[70] C. R. Barrett, W. D. Nix, and A. S. Tetelman, *The Principles of Engineering Materials* (Prentice-Hall, Englewood Cliffs, NJ, 1973), p. 197.
[71] Yu. G. Shreter, D. V. Tarkhin, S. A. Khorev, and Yu. T. Rebane, Phys. Solid State **41**, 1295 (1999).
[72] M. A. Grinfeld and Hazzeldine, Philos. Mag. Lett. **74**, 17 (1996).
[73] V. B. Shenoy, C. V. Ciobanu, and L. B. Freund, Appl. Phys. Lett. **81**, 364 (2002).
[74] A. Ramasubramanian and V. B. Shenoy, J. Appl. Phys. **95**, 7813 (2004).
[75] A. Witvrouv and F. Spaepen, J. Appl. Phys. **74**, 7154 (1993).
[76] W. W. Mullins and R. F. Sekerka, J. Appl. Phys. **35**, 444 (1964).
[77] N. Sridhar, J. M. Rickman, and D. J. Srolovitz, Acta Mater. **45**, 2815 (1997).
[78] R. Krishnamurthy and D. J. Srolovitz, J. Appl. Phys. **99**, 043504 (2006).
[79] R. M. Emrick and P. B. McArdle, Phys. Rev. **188**, 1156 (1969).
[80] M. W. Finnis and M. Sachdev, J. Phys. F: Met. Phys. **6**, 965 (1976).
[81] R. Kirchheim, Acta Metall. Mater. **40**, 309 (1992).
[82] R. Defay, I. Prigogine, and A. Bellemans, *Surface Tension and Adsorption* (Wiley, New York, 1966), p. 290.
[83] W. Barvosa-Carter and M. J. Aziz, Appl. Phys. Lett. **79**, 356 (2001).
[84] W. W. Mullins and R. F. Sekerka, J. Appl. Phys. **34**, 323 (1963).
[85] A. T. Huang, K. N. Tu, and Yi-S Lai, J. Appl. Phys. **100**, 033521 (2006).
[86] T. O. Ogurtani, A. Celik, and E. E. Oren, Thin Solid Films (to be published).
[87] T. O. Ogurtani and A. Celik, J. Appl. Phys. **100**, 043504 2006).
[88] E. Kröner, *Kontinuumstheorie der Versetzungen und Eigenspannungen* (Springer, Berlin, 1958).
[89] T. O. Ogurtani and A. K. Seeger, J. Appl. Phys. **66**, 5274 (1989).
[90] Q. Z. Hong, J. G. Zhu, J. W. Mayer, W. Xia, and S. S. Lau, J. Appl. Phys. **71**, 1768 (1992).